FERRITES

1. Introduction

The term ferrite is commonly used generically to describe a class of magnetic oxide compounds that contain iron oxide as a principal component. In metallurgy (qv), however, the term ferrite is often used as a metallographic indication of the α-iron crystalline phase.

Some representatives of the ferrite family have long been known as magnetic minerals. For example, magnetite [1317-61-9], Fe_3O_4, or loadstone (1) was known in ancient times, $\sim$400 BC, and magnetoplumbite [12173-91-0], $Pb(MNFe)_{12}O_{19}$ (2), has been known at least since the beginning of the twentieth century. The real breakthrough, however, of ferrites as important materials for electrotechnical applications took place in the early 1950s (3,4). This breakthrough built upon pioneering work in the mid-1930s (5,6) followed by the theoretical framework in 1948 (7).

Ferrites can be classified according to crystal structure, ie, cubic vs hexagonal, or magnetic behavior, ie, soft vs hard ferrites. A systematic classification as well as some applications are given in Table 1 (see also MAGNETIC MATERIALS, BULK; MAGNETIC MATERIALS, THIN FILMS AND PARTICLES).

The cubic ferrites, perovskite, garnet, and spinel, have quite different crystal structures and correspondingly different properties and applications. Perovskite ferrites, isostructural with the mineral perovskite [9003-99-0], $CaTiO_3$,

Table 1. **Systematic Classification of Ferrites**

Crystal chemistry[a]	Formula[b]	Magnetic nature: Soft	Magnetic nature: Intermediate	Magnetic nature: Hard	Appearance: Polycrystalline	Appearance: Single crystalline	Appearance: Bonded powder	Application
				Cubic				
spinel	$MeFe_2O_4$	X			X	X		recording heads
		X			X			core material for various inductors, transformers, and TV deflection units
	$CoFe_2O_4$, γ-Fe_2O_3		X				X	recording tape
garnet	RFe_5O_{12}		X			X		microwave, magnetooptics, bubble-information storage
perovskite	$R'FeO_3$					X		electroceramic devices
orthoferrite[c]	$RFeO_3$		X			X		bubble-information storage
				Hexagonal				
magnetoplumbite	$R'Fe_{12}O_{19}$			X[d]	X		X	permanent magnets
	$R'Fe_{12-x}Me'O_{19}$			X[e]			X	tape for perpendicular recording
W (= MS)	$R'Me_2Fe_{16}O_{27}$			X[d]	X		X	permanent magnets[f]
	$R'Co_2Fe_{16}O_{27}$		X[e]			X		microwaves, shielding[f]
X (= M_2S)	$R'MeFe_{28}O_{46}$			X[d]	X		X	permanent magnets[f]
	$R'CoFe_{28}O_{46}$		X[e]			X		microwaves, shielding[f]
Y (= ST)	$R'_2Me_2Fe_{12}O_{22}$		X[e]		X	X		microwaves, shielding
Z (= MST)	$R'_3Me_2Fe_{24}O_{41}$			X[d]				permanent magnets[f]
	$R'_3Co_2Fe_{24}O_{41}$		X[e]		X			microwaves, shielding

[a] M = $BaFe_{12}O_{19}$; S = $Me_2Fe_4O_8$; T = $Ba_4Fe_8O_7$. See Figure 1.
[b] Me = Fe^{2+}, Ni^{2+}, Mn^{2+}, Co^{2+}, Zn^{2+}, etc; Me′ = Mn^{3+}, (Ti^{4+} + {Co^{2+}), etc; R = Y, Nb, etc; R′ = Ba, Sr, Pb, Ca.
[c] These materials are orthorhombic.
[d] Preferred axis (uniaxial anisotropy).
[e] Preferred plane (planar anisotropy).
[f] Potential application.

contain iron in unusually high valency states, eg, +4, +5, +6 (8), giving rise to high and almost metallic electrical conductivity. Representatives are $(CaSr)FeO_3$ (8) and $(PbCa)Fe_2O_5$ (9). Applications are mainly in the field of electroceramic devices, eg, electrical transducers (see CERAMICS AS ELECTRICAL MATERIALS). Closely related to the perovskite ferrites are orthoferrites where the Ca is replaced by a rare-earth element, resulting in a distorted perovskite structure, which is essentially orthorhombic. Orthoferrites, studied extensively in the early 1970s as potential data storage materials based on magnetic bubble domains (10), had been largely replaced by the garnet materials (see INFORMATION STORAGE MATERIALS).

Garnet ferrites, isostructural with the mineral pyrope, $Mg_3Al_2Si_3O_{12}$, have a special feature. These materials can only accommodate trivalent iron together with trivalent rare earths. The absence of other valencies gives rise to extremely high electrical resistivity and very low losses in the microwave region (11). As single crystals, these are transparent and exhibit interesting magnetooptical properties (12). In addition garnet ferrites were the preferred bubble-domain data storage materials (13).

Spinel ferrites, isostructural with the mineral spinel [1302-67-6], $MgAl_2O_4$, combine interesting soft magnetic properties with a relatively high electrical resistivity. The latter permits low eddy current losses in ac applications, and based on this feature spinel ferrites have largely replaced the iron-based core materials in the radio frequency (rf) range. The main representatives are MnZn- ferrites (frequencies up to $\sim$3 MHz, such as the Ferroxcube 3F45 and 3F5 materials) and NiZn-ferrites (frequencies $\gg$ 3 MHz).

The soft magnetic spinel ferrites, by far the most important cubic ferrites, were first introduced by Philips under the trade name Ferroxcube (14) and are now widely commercially available under various trade names. The world market for soft magnetic ferrites amounts to about 650MUSD in 2002, $\sim$75 MUSD of which is in the United States.

Hexagonal ferrites cover a number of strongly related structures (Fig. 1) (15). The magnetization may be strongly bound to the hexagonal axis, the material exhibiting hard magnetic properties, or to the plane normal to this axis, such that the properties are mixed, ie, there is high permeability in the plane and low permeability in other directions. The group having mixed properties is called Ferroxplana (16). The hexagonal ferrites with uniaxial anisotropy are in principle interesting as permanent magnet material. However, W-, X-, and Z-type compounds (see Fig. 1) are not interesting economically because of relatively difficult processing.

Ferroxplana offer unique high frequency properties, being applicable where other high frequency materials such as NiZn ferrites fail (0.1–1 GHz). Some representatives are Co_2Z (17) and Zn_2Y (18). In spite of numerous investigations, application has always remained limited because of the difficult processing. Small-scale applications are in the field of microwaves (see MICROWAVE TECHNOLOGY) (19).

M-type ferrites, isostructural with the mineral magnetoplumbite, are by far the most important hexagonal ferrites. The M-type ferrites have a dominant position in the permanent magnet market, and are good candidates for another big volume market, ie, as base material for perpendicular recording tape. In

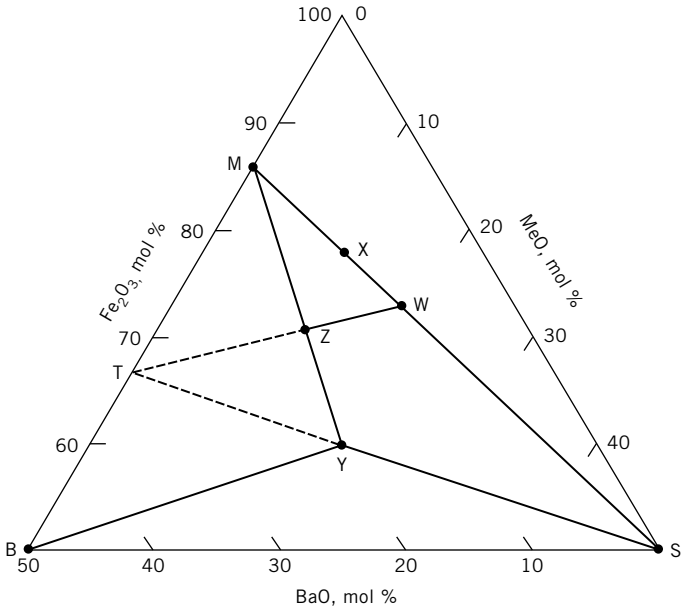

Fig. 1. Composition diagram for hexagonal ferrites where $B = BaFe_2O_4$, $M = BaFe_{12}O_{19}$, $S = MeFe_2O_4$, $T = BaFe_4O_7$, $W = BaMe_2Fe_{16}O_{27}$, $X = BaMeFe_{14}O_{23}$, $Y = BaMeFe_6O_{11}$, $Z = Ba_3Me_2Fe_{24}O_{41}$, and Me is as defined in Table 1.

addition there are some small-scale applications, eg, as microwave material at frequencies >20 GHz (19). Interest in barium-ferrite as a base material for particulate recording media has increased considerably since the invention of perpendicular recording in 1977. The Ba-ferrite medium is particularly suitable because it has a platelet crystallite shape with the preferred axis normal to the wide surface, thus allowing perpendicular alignment during the coating on the substrate film. Relatively low coercivity (~100 kA/m) and small (~50 nm) particle size are needed. This is realized by the partial substitution of Fe, eg, by using Co and Ti, and special powder preparation techniques. Despite promising characteristics (20,21), Ba-ferrite media have not found their way to the mass production market.

M-type ferrites are mainly used as permanent magnet material. They have largely replaced the alnicos as preferred permanent magnet material, as a result of the lower material and processing costs. These ferrites were first introduced under the trade name Ferroxdure, the isotropic form in 1952 (22) and the anisotropic (crystal oriented) form in 1954 (23), and are widely available commercially under various trade names. They cover ~57% of the world market of permanent magnet materials, corresponding to 4.8 billion U.S. dollars (1999), as well as 62% of the U.S. market, at $744 million (23).

More information on noncommercially available ferrites can be found in the literature (4,25). Extended reviews on soft (4,25–30) and hard (4,30–33) ferrites are also available. Explanations of magnetic concepts used in this article, such as permeability and coercivity, may be found in magnetism textbooks (34).

2. Common Properties of Spinel Ferrites and M-Type Ferrites

The commercial sintered spinel and M-type ferrites have a porosity of 2–15 vol% and a wide range in grain sizes (1–40 μm). In addition, these materials usually contain up to about 1 wt% of a second phase, eg, $CaO + SiO_2$ on grain boundaries, originating from impurities or sinter aids.

Ferrites are oxides and thus rather inert with respect to water, bases, and organic solvents. However, they may be attacked by acids having sufficiently high strength (pH <2), eg,

$$MeFe_2O_4(s) + 8\ HCl \longrightarrow Me^{2+} + 2\ Fe^{3+} + 8\ Cl^- + 4\ H_2O \qquad (1)$$

where Me is defined as in Table 1. The reaction rate is rather limited because of the low specific surface. However, the second phase on the grain boundaries, eg, CaO, may be more sensitive to acids and this may induce a more serious attack, the more so when there is open porosity, ie, when porosity >10 vol%. Being ceramic materials, ferrites are also resistant to high temperatures, at least up to the sintering temperature (1200–1400°C) (see CERAMICS). However, noticeable reduction may take place at temperatures >1100°C and an oxygen partial pressure, P_{O_2}, below the equilibrium oxygen partial pressure, as described by the relation

$$\log P_{O_2} = A/T + B \qquad (2)$$

where T is in kelvin and A and B are specific for each ferrite. M-ferrites can hardly change in oxidation degree and the P_{O_2}–T relation in fact represents the decomposition conditions (32). Spinel ferrites, however, allow considerable changes in the Fe^{2+} concentration without decomposition, but only accompanied by changes in the defect chemistry (27).

Ceramic ferrites cannot explode or release poisonous gases, and generally do not contain toxic elements. However, permanent magnets based on Sr-ferrite contain strontium [7440-24-6] , Sr, which is in principle toxic. In dense (porosity <10%) materials the Sr is firmly bound; however, in porous (porosity >10%) materials the second phase may dissolve partially in water or acids giving rise to release of Sr. Even in the latter case the effect is limited. Such magnets are used in the stomach of cows (pH <3) in order to collect iron-based particles eaten by the cow. Elements that can have different valencies, such as chromium, Cr; manganese, Mn; titanium, Ti; and vanadium, V, may be carcinogenic, in particular in the high valency state, eg, Cr^{6+}. Whereas these elements may be present in minor quantities in both hard and soft ferrites, generally they are firmly bound in the lattice and present in lower valency states. Nevertheless, upon chemical attack by an acid or during the preparation of those ferrites, some precautions are advisable.

3. Crystal Chemistry and Physical Properties

The magnetic properties of ferrites result from the electronic configuration and mutual interactions of the ions present. Thus investigation of the crystal

structure is fundamental to the understanding of these materials. Although the specific structures of spinel ferrites and M-type ferrites differ, both classes can be considered to be composed of two basic sublattices: An anionic lattice having relatively large anions in a closest packing and a cationic lattice containing the smaller cations, which fill interstitial sites.

3.1. Spinel Ferrites. In spinel ferrites having the composition AB_2O_4, where A and B are metals, cubic close-packed (CCP) oxygen ions leave two kinds of interstitial sites for the cations: tetrahedral or A-sites, surrounded by four oxygen ions; and octahedral or B-sites, surrounded by six oxygen ions. Figure 2 gives a schematic impression. The smallest crystallographic unit cell having the required symmetry contains eight formula units of AB_2O_4. Each unit cell has 64 tetrahedral sites, eight of which are occupied, and 32 octahedral sites, 16 of which are occupied. A wide variety of transition-metal cations can be fit into these interstitial sites. The most important family of spinels is $Me^{2+}Fe^{3+}{}_2O_4$, where Me = Mg, Mn, Fe, Co, Ni, Zn, Cu, etc, either singly or in combination. But similar ferrites having less than two Fe-ions per formula unit are also of industrial significance because of the high electrical resistivity.

The site preference of several transition-metal ions is discussed in Refs. 4 and 25. The occupation of the sites is usually denoted by placing the cations on B-sites in structure formulas between brackets. There are three types of spinels: normal spinels, where the A-sites have all divalent cations and the B-sites all trivalent cations, eg, Zn-ferrite, $Zn^{2+}[Fe^{3+}{}_2]O_4$; inverse spinels where all the divalent cations are in B-sites and trivalent ions are distributed over A- and B-sites, eg, Ni-ferrite, $Fe^{3+}[Ni^{2+}Fe^{3+}]O_4$; and mixed spinels, where both divalent and trivalent cations are distributed over both types of sites, eg, Mn-ferrite $Mn^{2+}{}_{0.8}Fe^{3+}{}_{0.2}[Mn^{2+}{}_{0.2}Fe^{3+}{}_{1.8}]O_4$.

In the cases of existing unpaired *d* electrons, transition-metal ions possess a net magnetic moment. In a spinel, these magnetic moments interact through the anions (super exchange), resulting in a situation where the moments of both A- and B-site ions are aligned, ie, A—A and B—B parallel, but A—B antiparallel, a ferrimagnetic ordering. The net magnetic moment per unit formula can be calculated from the distribution of the cations over these sites. For example,

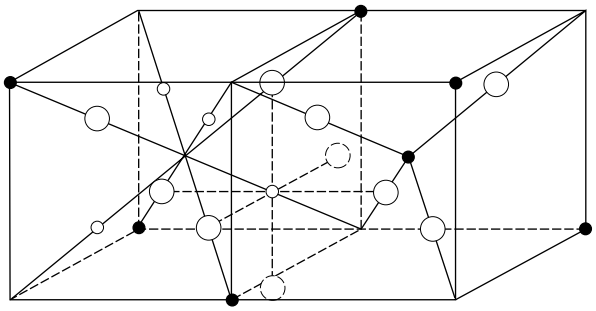

Fig. 2. Spinel structure where (←--→) is oxygen, ●, A-sites, ○, B-sites. A unit cell consists of eight face-centered cubic (fcc) subcells with different cation occupants. Adapted from Ref. 4.

the inverse spinel $Fe^{3+}[Ni^{2+}Fe^{3+}]O_4$, where Fe^{3+} and Ni^{2+} have five and two unpaired electrons, respectively, has a magnetic moment of 5 Bohr magnetons, μ_B, on the A-site sublattice and a magnetic moment of $5+2=7\mu_B$ on the B-site sublattice. The opposite alignment of the two sublattices yields a net magnetic moment of 2 μ_B per formula unit. Because $1\mu_B = 1.1653 \times 10^{-29}$ Wb · m, there are eight formula-units per cell, and the lattice constant is 8.34×10^{-10}m, it can easily be calculated that this corresponds to a value for the saturation induction, B_s, of 0.32 tesla at 0 K. This is reasonably near the measured value of 0.35 tesla (Fig. 3). In comparing these data, it is assumed that all magnetic domains, in each of which the ferrimagnetic ordering holds often over many thousands of unit cells, are perfectly aligned by a strong applied magnetic field.

It is possible to systematically alter the net magnetic moment of ferrites by chemical substitutions. A very important industrial application is the increase of the magnetic moment in mixed MnZn-ferrites and NiZn-ferrites. When Zn ions are introduced in Mn-ferrite or Ni-ferrite, these ions prefer to occupy A-sites. Because Zn^{2+} is nonmagnetic, the A-sublattice magnetization is reduced and consequently the total net magnetic moment is increased. Figure 3**a** shows that for smaller Zn contents, magnetic data follow the expected relationships. However, high Zn content causes the net moments to decrease because some of the Fe^{3+} ions no longer have magnetic neighbors and interactions break up. Another decrease of the degree of magnetic moment alignment occurs when temperature is increased Figure 3**b** shows the influence of thermal agitation. At a certain temperature, the Curie temperature T_c, the magnetic ordering completely vanishes.

The direction of the alignment of magnetic moments within a magnetic domain is related to the axes of the crystal lattice by crystalline electric fields and spin-orbit interaction of transition-metal d ions (24). The dependency is given by the magnetocrystalline anisotropy energy E_a expression for a

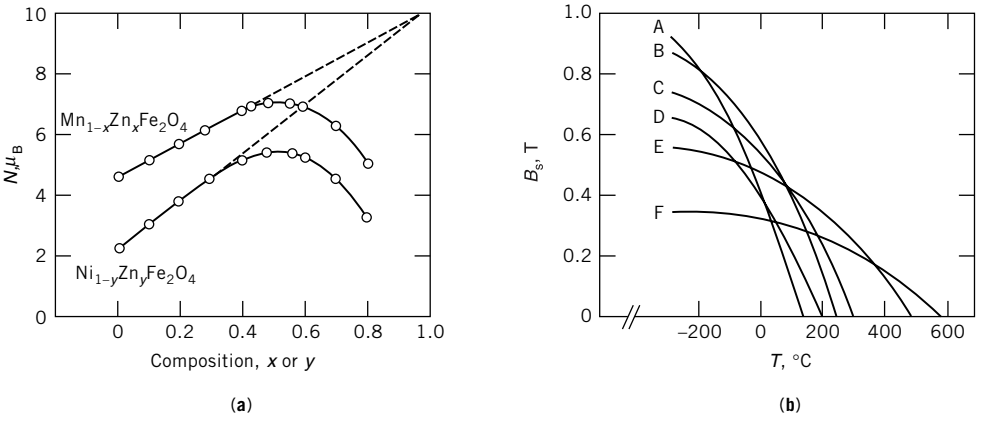

Fig. 3. (**a**) Saturation magnetic moment per formula unit, N, in Bohr magnetons vs chemical composition at 0 K and (**b**) saturation magnetic induction, B_s, in teslas vs temperature for mixed ferrites $Mn_{1-x}Zn_xFe_2O_4$ and $Ni_{1-y}Zn_yFe_2O_4$ where A, B, and C represent $x = 0.5, 0.15$, and 0, respectively, and D, E, and F represent $y = 0.65$, 0.2, and 0, respectively. To convert μ_B to J/T, multiply by 9.274×10^{-24}. Adapted from Ref. 4.

cubic lattice (34):

$$E_a = K_1\left(\alpha_1^2\alpha_2^2 + \alpha_1^2\alpha_3^2 + \alpha_2^2\alpha_3^2\right) + K_2\alpha_1^2\alpha_2^2\alpha_3^2 + \cdots \quad (3)$$

where the α_i are direction cosines of the magnetization with respect to the three principal crystal axes and K_i are phenomenological anisotropy constants. The lowest order terms are the most relevant ones; terms higher than ${\alpha^6}_i$ can be neglected. The constants K_1 and K_2 can be determined by measuring the torque exerted on a monocrystalline sample sphere by a rotated saturating magnetic field (34).

Figure 4 shows a typical result for K_1 as a function of temperature for a Fe^{2+}-containing MnZn-ferrite. K_1 changes sign at a certain temperature T_0 because the positive contribution from the Fe^{2+} ions compensates the negative contributions from the other ions (25,35,36). From the expression for E_a it can be derived that the preferred direction of the magnetization changes from [111] to [100] at the temperature where $K_1+(1/9)K_2 = 0$. This is not far from T_0 (36). Near T_0 the direction of the magnetization can easily be changed by applying just a small magnetic field H. In other words, the initial magnetic permeability $\mu_i = \mathrm{B}/(\mu_0 \cdot \mathrm{H})$, where B is the resulting net macroscopic magnetic induction and $\mu_0 = 4\pi \times 10^{-7}$ Wb/(A · m), is high in that region (Fig. 4**a**). The vanishing anisotropy near the Curie temperature leads to the so-called primary maximum in $\mu_i(T)$; the maximum at T_0 is known as the secondary maximum.

The net macroscopic B and the resulting μ_i result from two types of magnetization processes. First, there is a contribution from the rotation of the magnetization inside each individual magnetic domain, from the preferred direction toward the direction of the applied magnetic field until the sum of the magnetostatic energy (minimal if B lies along H) and the anisotropy energy has reached its minimum value. Second, domain walls move. Domains having favorable magnetization directions with respect to the applied magnetic field grow at the expense of others, thus further minimizing the total magnetostatic energy. In view of the small magnitude of the applied field H, irreversible jumps of domain walls from pinning points such as grain boundaries, internal pores, or inclusions do not take place, but small reversible motions may readily occur. The extent to which each of the two mechanisms contribute to μ_i depends on quite a number of parameters: chemical composition, temperature, ceramic microstructure, stresses, frequency of H-field, etc. As for the microstructure, grain boundaries often play an essential role because of pinning of domain walls. The effective initial permeability depends more or less linearly on grain size (37,38). In small grains the rotational contribution dominates, whereas at increasing grain sizes the wall contribution becomes more and more important. A review of experimental data and recent theoretical models can be found in (39).

Stresses, which can, eg, be introduced during cooling after ceramic sintering, during machining of sintered products, or simply when product parts are clamped together before use, lead to anisotropy by the magnetostriction effect (25,34,40). The influence of stress anisotropy can be large in cases of a small magnetocrystalline anisotropy, ie, in the regions of the $\mu_i(T)$ maxima, resulting in a considerable suppression of the maxima and sometimes even of the whole curve.

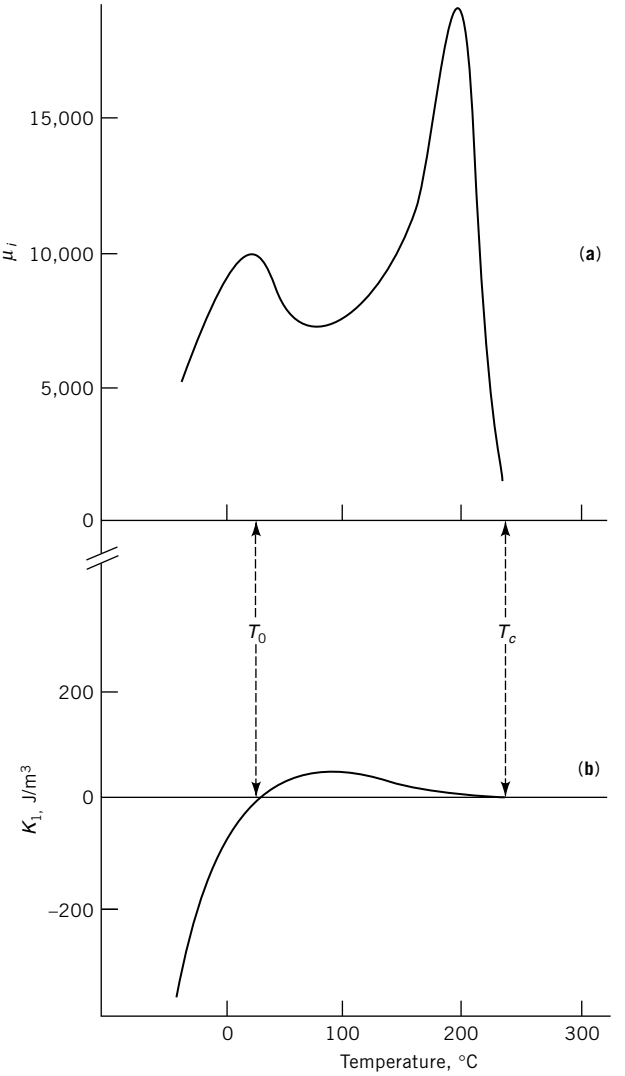

Fig. 4. The effect of temperature for $Mn_{0.6}Zn_{0.3}Fe^{2+}{}_{0.1}Fe^{3+}{}_2O_4$ on (**a**) initial magnetic permeability, μ_i, measured on a polycrystalline toroid applied as a core for a coil driven by a low ($B < 0.1$ mT) amplitude, low (10 kHz) frequency sinusoidal signal; and (**b**) magnetocrystalline anisotropy constant, K_1, measured on a monocrystalline sphere showing the anisotropy/compensation temperature T_0 and the Curie temperature, T_c. To convert joules to calories, divide by 4.184.

Magnetocrystalline anisotropy, magnetostriction, and magnetic permeability depend markedly on chemical composition. These dependencies have been extensively investigated within the ternary diagrams $MnFe_2O_4$–Zn-$ZnFe_2O_4$–Fe_3O_4 and $NiFe_2O_4$–$ZnFe_2O_4$–Fe_3O_4 (34,35,40,41). The saturation induction B_s and Curie temperature T_c are also composition dependent (41–43) as is the electrical resistivity, which varies markedly. Spinel ferrites are

semiconductors (qv) (25). In case of an excess of iron appearing as Fe^{2+}, the conduction is of the *n*-type where electrons hop between different Fe ions. The resistivity then is usually much smaller than for Fe-deficient ferrites. This relatively high (0.1 $\Omega \cdot m$ to $10^8 \Omega \cdot m$ at 25°C) dc resistivity is very important.

Properties can also be manipulated by adding specific dopants: Co^{2+} ions are, eg, introduced for extra anisotropy compensation (25,44–46); and Ti^{+4} ions are substituted to form pairs with Fe^{2+} ions and thus to reduce electron hopping (46,47). Extensive investigations (48–51) have been carried out involving the addition of dopants such as CaO (typically 0.1 mol%) and SiO_2 (0.01 mol %) in order to provide ceramic grains having electrically insulating grain boundaries, thus markedly increasing the effective resistivity of the ferrite product.

At high frequencies, ferrites exhibit energy losses resulting from various physical mechanisms at different frequencies and appearing as heat dissipation. Hysteresis losses arise from irreversible domain wall jumps. During each cycle of the *H*- and *B*-fields one hysteresis loop is completed and the loss per cycle is proportional to the area of the loop. A way to reduce hysteresis losses, ie, prevent domain wall jumps, is to reduce the number of inhomogeneities able to pin domain walls, eg, pores and impurities, and to reduce magnetocrystalline and stress anisotropy (52,53). Another method is to deliberately pin the walls, for instance by addition of Co^{2+} and Ti^{4+} ions or by using ceramic microstructures having small grains (54,55). A second important loss contribution comes from eddy currents, induced by alternating magnetic fluxes. This contribution can be limited by providing a high electrical resistivity (56,57). At high frequencies, this is not easy at all, because insulating grain boundaries tend to become short circuited as a result of the permittivity of the ferrite (29). A third main loss contribution is from magnetic resonances. Above ~1 MHz, this is usually the

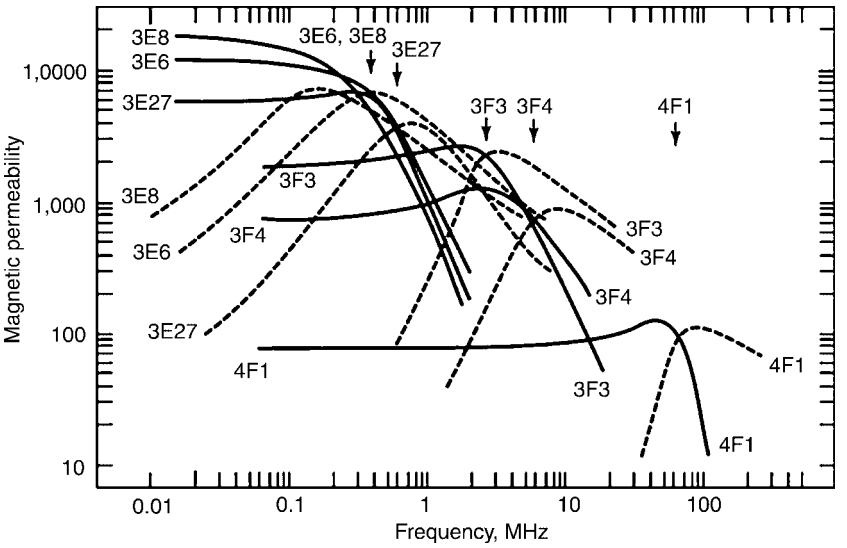

Fig. 5. Complex magnetic permeability vs frequency for a series of ferrites used for power transformers and inductors at 25°C, $B < 0.1$ mT: (—) represents real parts μ', (---) show the imaginary parts μ''. The arrows indicate the frequencies where $\tan\delta = \mu/\mu' = 1$ (58).

dominant contribution. When the driving frequency is in resonance with the natural frequency at which the magnetization rotates, there is a large peak in power absorption. This effect can be seen when the magnetic permeability is considered as the complex parameter $\mu = \mu' + j\mu$. The ratio μ''/μ' is usually expressed as tan δ, where δ is the so-called loss angle, the phase-lag of the magnetic induction with respect to the applied magnetic field. For inductors in electrical circuits, δ expresses the phase difference between voltage and current. Figure 5 shows μ'

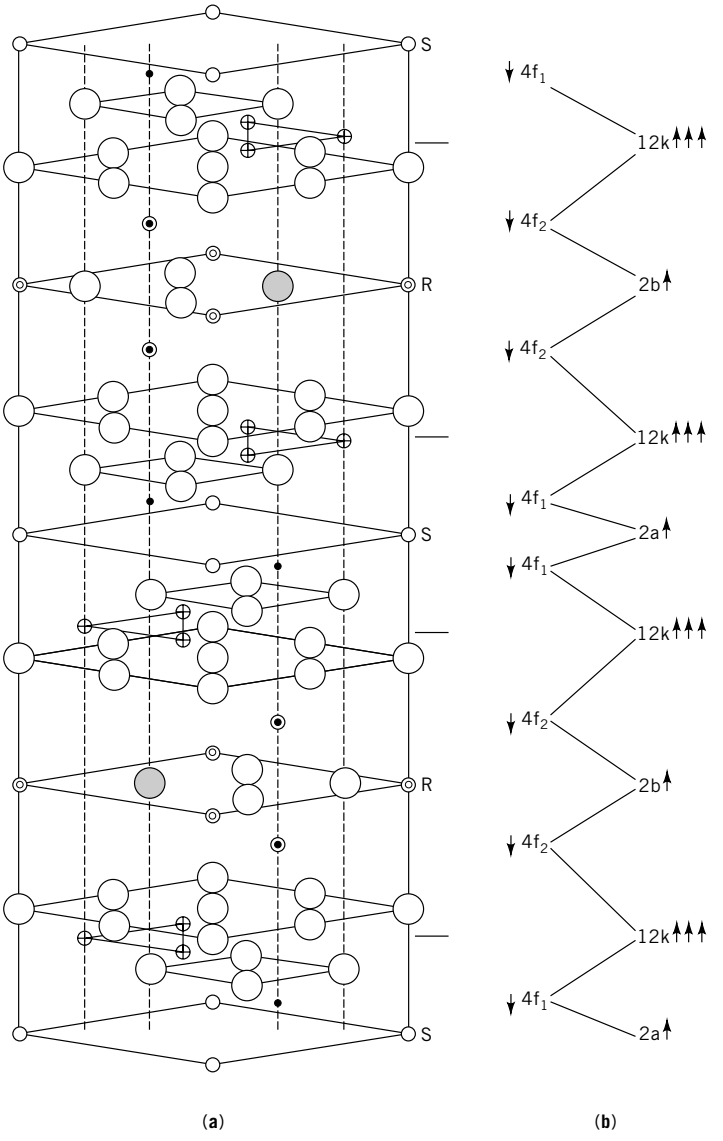

Fig. 6. The M-ferrite (**a**) crystal structure showing the S and R subunits where ○ is O^{2-}; ◉, Ba^{2+}; and ●, ●, ○, •, and are all Fe^{3+} at 12k, $4f_2$, $4f_1$, 2a, and 2b positions, respectively; (**b**) magnetic structure where the arrows represent size and spin direction of unpaired electrons at the various crystallographic positions.

and μ'' as functions of frequency for some commercial ferrites. These ferrites show large differences concerning the frequencies where μ'' starts to come up and accordingly, in the resonance frequencies, where $\tan \delta = 1$. But, also, the low frequency permeabilities differ. The resonance frequency is inversely proportional to the low frequency permeability (59). Applying this, shifting resonance to high frequencies can be realized by small grain sizes. The ferrites of Figure 5 are optimized for a range of frequencies and induction levels (58).

3.2. M-type Ferrites. The M-structure borrows its name from the lead-containing magnetic mineral magnetoplumbite on which this structure was based in 1938 (60). Once the technical importance of M-ferrites had become clear, the structure of $BaFe_{12}O_{19}$ was determined in more detail, together with the related structures of other hexagonal ferrites (61). Figure 6 shows the unit cell of the M-structure, which corresponds to two formula units. Its symmetry is characterized by the space group $P6_3/mmc$. The structure shows a closest hexagonal packing of O ions, where 2 of the 40 sites are occupied by Ba-ions; Fe-ions are in interstitial sites. The structure is built up from smaller units: a cubic block, S, having the spinel structure and a hexagonal block, R, containing the Ba ions. The Fe ions are located at five different crystallographic positions; cell dimensions and theoretical densities are given in Table 2 (60,62,63). Various substitutions are possible in $BaFe_{12}O_{19}$ (31). Some important isovalent substitutions are Sr and Pb for Ba; and Mn, Al, and Cr for Fe. If the substituting ion does not have the same charge, the charge must be compensated (pair substitutions), eg, $BaFe_{12-x}Fe_x^{2+}O_{19-x}F_x^-$, and $BaFe_{12-2x}Ti_x^{4+}Co_x^{2+}O_{19}$.

The magnetism of $BaFe_{12}O_{19}$ comes from the Fe^{3+} ions, each carrying a magnetic moment of 5 μ_B. These are aligned by either parallel or antiparallel ferromagnetic interaction. Ions of the same crystallographic position are aligned parallel, constituting a magnetic sublattice. The interaction between neighboring

Table 2. **Properties of M-Ferrites**[a]

Parameter	Ferrite[b] BaM	SrM	PbM
Crystallographic properties			
lattice constants, nm			
A	0.5893	0.588	0.588
C	2.3194	2.307	2.302
molecular weight	1112	1062	1181
density, g/cm^3	5.28	5.11	5.68
reference	61	59	62
Primary magnetic properties			
saturation magnetization, J_s, mT	478	478	402
σ_s, μV sm/kg	90.4	93.4	70.8
anisotropy constant[d], K_1, kJ/m^3	330	360	220
Curie temperature, T_c, K	740	750	725
reference	63	63	64

[a] Measurements are at room temperature.
[b] $M = Fe_{12}O_{19}$.
[c] The exchange energy coefficient, A, is 5.1×10^{-12} J/m (1.2×10^{-12} cal/m) (65).
[d] To convert joules to calories, divide by 4.184.

ions of different sublattices is a result of superexchange by oxygen. The theory predicts that the atomic moments are parallel when the Fe−O−Fe angle is about 180° and antiparallel when this angle is about 90° (4). The most probable magnetic structure, consisting of five sublattices, is represented schematically in Figure 6 (66). Its verification was first based on the measurement of the saturation magnetization. Additional experimental evidence was obtained from electron diffraction analysis (67) and Mössbauer spectroscopy (65). Recently, it is also supported theoretically by an *ab initio* calculation (68). It is the magnetic structure in terms of sublattices and their mutual orientation that governs magnetic behavior, which in turn is described in terms of intrinsic and material properties.

The intrinsic magnetic properties may be subdivided into primary and secondary. The primary properties are directly related to the magnetic structure; the secondary properties, derived from the primary ones, govern the actual magnetic behavior.

The *primary* intrinsic magnetic properties are the saturation magnetization J_s, the magnetocrystalline anisotropy constant K_1 and the exchange constant A. Room Temperature (RT) values are given in Table 2, while the temperature behavior is shown in Fig. 7.

The saturation magnetization, J_s, is the (maximum) magnetic moment per unit of volume. It may be derived from the spin configuration of the sublattices: eight ionic moments and, hence, 40 μ_B per unit cell, which corresponds to

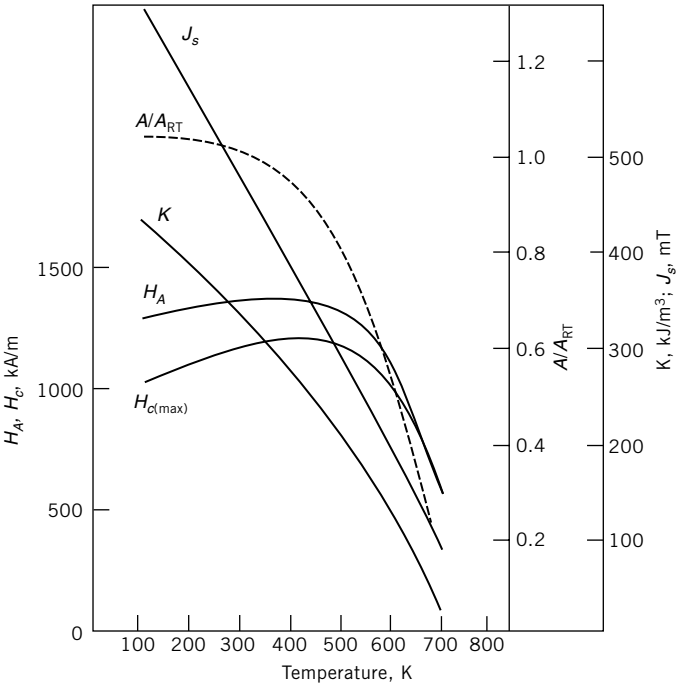

Fig. 7. Temperature dependence of J_s, K_1, H_A, and H_c(max) for (—) BaM (4) and of A for (– – –) PbM (69). See text. To convert joules to calories, divide by 4.184.

$J_s = 668$ mT at 0 K. This was the first experimental support for the Gorter model (66). The temperature dependence of J_s (Fig. 7) is remarkable: the J_s-T curve is much less rounded than the usual one, as derived from a Brillouin function (33). This results in a relatively low J_s value at RT (Table 2) and a relatively high temperature coefficient of J_s (-0.2% °C). By means of Mössbauer spectroscopy, the temperature dependence of the separate sublattice contributions has been determined (65). It appears that the 12k sublattice is responsible for the quasilinear temperature dependence of the overall J_s.

The exchange energy coefficient A characterizes the energy associated with the (anti)parallel coupling of the ionic moments. It is directly proportional to the Curie temperature T_c (70). An experimental value for A (Table 2), as well its temperature dependency (Fig. 7) has been derived from domain-width observations on PbM (69). It appears that A is rather constant in the low temperature region up to 300°C. Because the Curie temperatures and the unit cell dimensions are rather similar, about the same values for A are expected for BaM and SrM.

The magnetocrystalline anisotropy constant K_1 is related to the preference of the magnetization to the hexagonal c axis. This is usually attributed to spin–orbit coupling of the Fe-ions, in particular on the 2b sites (71). The energy associated with this phenomenon is characterized by K_1. Higher order constants (K_2, K_3) are negligibly small. The temperature behavior (Fig. 7) is more or less similar to that of J_s.

The *secondary* intrinsic magnetic properties characterize the actual magnetic state. The latter minimizes the three energies involved: the exchange energy, E_e, the anisotropy energy, E_a, and the magnetostatic energy, E_m, being governed by the values of A, K, and J_s, respectively. Some main secondary properties are given in Table 3.

The specific wall energy, γ_w, represents a combination of both E_e and E_a, because walls are present to reduce E_m, but their internal structure is not favorable for E_e and E_a.

The critical diameter for single-domain behavior, D_c, is the diameter below which magnetic domains are unfavorable in an isolated spherical particle. Although M-ferrite particles are not spherical and magnetostatic interactions between the particles also play a role, D_c remains an important indicator for the grain size needed in high quality magnets. In the absence of domains magnetization reversal proceeds by rotation.

Table 3. **Secondary Magnetic Properties for SrM**[a]

Parameter[b]	Definition	Value
specific wall energy,[c] γ_w, J/m^2	$4(AK)^{1/2}$	54.2×10^{-4}
critical diameter single-domain behavior, D_c, μm	$18\mu_0\gamma_w J_s^{-2}$	0.54
anisotropy energy/magnetostatic energy, E_a/E_m	$2\mu_0 K J^{-2}$	4.0
anisotropy field, H_A, kA/m	$2\ K J_s^{-1}$	1506
maximum coercivity, H_c(max), kA/m	$H_A - N J_s \mu_0^{-1}$	1240

[a] $A = 5.1 \times 10^{-10}$ J/m, $K = 360$ kJ/m^3, $J_s = 478$ mT (Table 2).
[b] Self-demagnetizing factor of crystals $N = 0.7$; $\mu_o = 4\pi \times 10^{-7}$ Wb//(A·m).
[c] To convert joules to calories, divide by 4.184.

The ratio E_a/E_m determines whether rotation is coherent or not. For M-ferrites, where $E_a/E_m > 0.36$, rotation is completely coherent (70).

The anisotropy fieldstrength, H_A, is the maximum internal reverse field-strength needed for magnetization reversal by coherent rotation. It corresponds also to the perpendicular field needed to turn the magnetization perpendicularly to the preferred c axis (4).

The maximum coercivity $H_{c(\max)}$ corresponds to H_A, but refers to the external field. It explicitly takes into account the self-demagnetizing field of the crystal (NJ_s/μ_0) as governed by the self-demagnetizing factor N. The latter ranges from 0 (for needles) to 1 (for thin plates). For platelet-shaped M-ferrite crystals N ranges from 0.6 to 0.9. $H_{c(\max)}$ represents an upper limit for the coercivity of an aligned assembly of noninteracting crystals and 0.48 $H_{c(\max)}$ the same for an isotropic assembly (72). Real coercivity values are much smaller resulting from the formation of transient domains and magnetostatic interactions.

The temperature dependence of H_A and $H_{c(\max)}$ is also shown in Figure 7. H_A appears to increase slightly and $H_{c(\max)}$ to increase clearly up to 300°C, implying a positive temperature coefficient for the coercivity. This is indeed observed, although $H_{c(\max)}$ describes only an idealized case.

Substitution may affect the intrinsic properties (32). Ba can be fully replaced by Sr or Pb and partly by Ca (<40 mol%). CaM, stabilized with 0.03 mol % La_2O_3, is also possible. The intrinsic properties of these M-ferrites vary somewhat and other factors such as sintering behavior and price of raw materials often dictate the commercial viability. Large-scale production is concentrated on BaM and SrM. High performance magnets are based on SrM, and cheap magnets are usually based on BaM. Recently, a new generation of high performance magnets have come to the stage, based on partial substitution of Sr^{2+} by La^{3+} compensated by Co^{2+}($+Fe^{2+}$) at the Fe sites (73–75).

Substitution for Fe^{3+} has a drastic effect on intrinsic magnetic properties. Partial substitution by Al^{3+} or Cr^{3+} decreases J_s without affecting K_1 seriously, resulting in larger H_A and H_c values. Substitution by Ti^{4+} and Co^{2+} causes a considerable decrease in K_1; the uniaxial anisotropy ($K_1 > 0$) may even change into planar anisotropy ($K_1 < 0$). Intermediate magnetic structures are also possible. For example, preferred directions on a conical surface around the c-axis are observed for In^{3+} substitution (76). For a few substitutions the K_1 value is increased whereas the J_s value is hardly affected, eg, substitution of Fe^{3+} by Ru^{3+} (77) and notably by Co^{2+} or Fe^{2+} when compensated by La^{3+} at Ba-sites (71,78–80).

The magnetic material properties are characterized by the J–H loop and in particular by the demagnetization curve. The latter, in turn, is characterized by the two end points, remanence B_r and coercivity H_{cJ}, as well as by its squareness. Remanence and coercivity are governed by the intrinsic properties, but also by a number of microstructural factors such as grain size and shape, volume fraction of ferrite phase, and alignment.

The remanence is given by the next expression, holding for medium and high grade materials where domains are absent in the remanent state:

$$B_r = f(d/d_x)s \cdot J_s \qquad (4)$$

where f is the degree of alignment: (d/d_x) the relative density, hence, the volume fraction of the solid; and s the fraction of pure ferrite in the solid. Typical values are $f = 0.5$ (isotropic) and $f = 0.9$ (anisotropic); $(d/d_x) = 0.9$ (sintered) and 0.6 (plastic bonded); $s = 0.96$. For high B_r material such as that used for loudspeakers, high density and high alignment are crucial. Equation 4 shows also that the relative temperature coefficient (TC) of B_r is equal to that of J_s(0.2% K).

The coercivity mechanism is related to the grain size. Typical anisotropic sintered materials have a grain size of 1 μm, ie, somewhat larger than D_c, but sufficiently small to avoid domains down to considerable counter fields. Magnetization reversal proceeds by nucleation and growth of (transient) domains (81). On a macroscale the reversal process is nonuniform, being governed by the initiation and growth of multicrystal reversed regions (82). On this basis, the next expression for the coercivity has been proposed (82):

$$H_{cJ} = aH_A - bJ_s/\mu_0 = H_n - N(B_r + J_s)/\mu_0 \qquad (5)$$

where the first term represents the average internal field (H_n) needed to nucleate a reversed domain. The coefficient a ranges from 0 to 1 and depends mainly on the grain size. The second term represents the effect of internal demagnetizing fields. The coefficient b ranges from 0 to 2 and is governed by the crystal demagnetizing factor N and, hence, by the crystal shape. The expression for the coercivity explains also the TC of the coercivity, known to be $\sim$1 kA/m.K. Although this coercivity expression has been derived for anisotropic sintered materials, it appears to apply also to isotropic ones (83).

For plastic-bonded materials, no clear-cut expression for the coercivity is known. It may be expected that it is rather similar, but with a smaller influence of B_r. For loosely packed fine powders the coefficient a approaches the theoretical value 0.48 (73). In all cases, high coercivity is obtained by using small grains with limited plate-like shape, ie, the value of N is not too high.

The performance of a magnet is characterized by a combination of B_r and H_c. For static applications at high B/μ_oH, the $(BH)_{\max}$ value can be used. For dynamic applications, however, $(BH)_{\max}$ is less indicative, because it is hardly sensitive or even insensitive to improved H_c values. In that case, the product of B_r and H_{cJ} is more suited (84). The parameter IP(mT) $= B_r + 0.4\ \mu_o H_{cJ}$ is a measure for the processing quality (costs). It is in practically independent of the firing temperature and the Al^{3+} or Cr^{3+} content by which the B_r/H_{cJ} ratio can be varied, while the powder processing remains equivalent.

Physical properties other than magnetic ones are summarized in Table 4, including the influences of porosity and of the measuring direction, ie, parallel ($||$) or perpendicular ($\perp$) to the preferred axis. Nearly all properties are clearly anisotropic, the ratio between both values being $\sim$2. For application, the mechanical tensile strength is most important. It is very sensitive to microstructural factors and to the measuring method. For that reason there is always a large scatter in measuring results. Mostly, the flexural strength is measured instead of the tensile strength because the scatter in results is less. The intrinsic material strength depends on overall factors, such as porosity, second phase, and internal stress level. The latter is considerable when, upon cooling from sintering, the anisotropic thermal shrinkage is not free in both directions, eg, in the

Table 4. **Other Physical Properties of BaM and SrM**

Property	Value ⊥	Ratio ∥/⊥	M-ferrite Ba	M-ferrite Sr	Remarks	References
Vickers hardness, GPa	5.6	1.5		X	depends on porosity	78
strength, MPa						
1. tensile (drawing test)	73	0.5	X		depends on porosity	77
2. flexural (bending test)	178–255	≅0.65		X	sensitive to imperfections and	79
3. compressive	785			X	measuring method	80
Young's modulus, GPa	211–317	1.2–2.0	X		depends on porosity	77,81
thermal expansion coefficient, K^{-1}	10^{-5}	1.4	X	X	depends slightly on temperature until T_c	77
electrical resitivity, Ωm	10^{-2}–10^{-6}	0.1	X		depends on $[Fe^{2+}]$	31
heat capacity		840 Jkg · K		X		4
thermal conductivity		6.3 W/ m · K		X		4

case of radially oriented rings (85). The actual strength of a product depends also on local factors such as inhomogeneities in density, alignment, grain size, and the presence of initial cracks. For complicated products, such as motor segments (arcs), the local factors are often predominant.

4. Processing

Commercial ferrites are produced by a ceramic process involving powder preparation, shaping, firing, and finishing (see CERAMICS, OVERVIEW). The powder preparation is usually the classical one involving the mixing of powder raw materials, prefiring (or calcination), milling, and granulating. The raw materials are oxides or carbonates, the main component always iron oxide. The morphology and purity of the raw materials are an important factors with respect to the processing and final quality (86). Mixing can be done in different ways, depending on the nature and quality of raw materials and of the final product. During prefiring the different compounds react in the solid state to form the final compound and intermediate compounds, loosing the volatile substances such as CO_2. Mostly this process is accompanied by homogenization on a local scale. In addition, there is some densification. To limit the effect of densification and to facilitate the handling of the material, it is often granulated before prefiring. To enable shaping and sintering, the prefired material has to be milled down to micrometer-sized particles. The last milling step is generally wet milling to prevent agglomeration effects. During or after milling, binders and lubricants are usually added to facilitate granulating and pressing.

In some cases, it may be advantageous to deviate from the classical technology. For example, in wet-chemical preparation better chemical and morphological control may be achieved by starting from salt solutions.

Shaping is often done by dry pressing, which in fact is a simple and effective method to make the variety of shapes needed for electronic applications. Dry pressing requires a drying and granulating step after wet milling. For high grade M-type ferrites, usually wet pressing is applied for reasons related to the field aligning of the powder particles. Special shaping techniques such as injection molding, extrusion, and isostatic pressing may be applied to realize special shapes or high performance products.

During firing, formation of the proper compound is completed and densification occurs from ~50 to ~90% solid by volume, implying a linear shrinkage of 10–25%. This shrinkage has to be anticipated by the pressing dimensions, constituting the shrinkage allowance. During the sintering process grain growth also occurs. Because the grain size and the grain boundary state are key factors for establishing the final electrical properties, control of grain size and grain boundaries is crucial. Generally a main factor is control of the second phase by ensuring the purity of raw materials and milling additives.

Pressing and sintering together determine the size and shape of the final product, but these are not well controlled with respect to the critical parts which determine the airgap in the magnetic circuit. For that reason a finishing touch by machining is necessary.

4.1. Spinel Ferrites. Prefiring is usually carried out in an air atmosphere in a continuous rotary kiln. In such a kiln the material is transported through a heat zone typically of 900–1100°C, in a rotating tube inclined at a small angle, which transports the powder downward along its length by a tumbling action. The angle is predesigned for a proper heating time and an economical throughput. When the mixture of raw materials enters the heat zone, carbonates and higher oxides decompose and a sequence of solid-state reactions occurs, starting with the formation of Zn-ferrite and ending with the partial formation of the desired MnZn-ferrite or NiZn-ferrite (87,88). Usually, the aim is not a 100% spinel structure after prefiring. A 50–80% one usually suffices because the remaining conversions take place during the final sintering step after the forming step. Too high prefiring temperatures would result in considerable shrinkage in this stage, which makes the ferrite hard and thus difficult to mill. The prefired powder is characterized by X-ray diffraction, by the BET specific surface or the Fisher number, and sometimes by the inductance of a coil wound on a toroid pressed from the prefired powder. The prefired and subsequently milled powder has to be such that it results in a predictable and very constant shrinkage of pressed products during final sintering, in order to satisfy tight demands normally imposed on final product dimensions or to be able to realize these dimensions by grinding.

Dry pressing requires free-flowing spherical granules. These granules are usually made by spray drying slurries of 50–80 wt% ferrite in water, to which 1–4 wt% organic binder, eg, an acrylate or poly(vinyl alcohol) and a dispersant, eg, polyethylene glycol, are added (see DISPERSANTS). In this process, the slurry is sprayed and atomized into droplets, which are subsequently dried in whirling hot air and collected as dry granules. To enhance the flowability, a lubricant such as zinc stearate or ammonium stearate is often added before or after spray drying. The granules must be solid enough to prevent the formation of dust during transportation, but must easily deform during pressing to facilitate

good compaction. Granule sizes are usually in the 50–500-μm range depending on the size and the geometry of the products to be pressed. Applied pressures are 50–150 MPa (7,250–21,750 psi) typically, depending on size and geometry of the products to be pressed, resulting in pressed densities of the order of 2–3 g/cm^3.

If products having large aspect ratios, eg, relatively long products with small cross-sections, have to be pressed, powder—wall friction tends to result in locally low pressed densities. Abrupt changes of cross sections can also give rise to considerable density gradients. The result can be serious product deformation during sintering—shrinkage. These gradients can be reduced by compressing granulates from two sides by moving the die in the direction of the punch. In addition, powder—wall friction can be reduced by die wall coating, applying a thin, very smooth, wear-resistant layer.

The choice of the granulate binder system is also determined by the desirability of obtaining a high green strength of the pressed products in order to facilitate handling without damage and by the necessity of avoiding residues after binder burnout.

Binder burnout is usually the first part of the final firing cycle. Its execution is quite critical since it is also related with the phase composition of the ferrite material (89). In this cycle, spinel structure formation is completed, shrinkage and formation of microstructure take place, and multivalent ions are given the desired valencies. Thus the final mechanical, electrical, and magnetic properties of the ferrite are determined. This firing is performed in large, very precisely computer-controlled kilns, which may be either continuous tunnel kilns through which the ferrite products travel or stationary batch kilns. NiZn-ferrites can usually be sintered in a simple constant atmosphere like air or nitrogen. MnZn-ferrites, however, especially those designed to contain Fe^{2+} ions, require sophisticated computer control of atmosphere during firing. The Fe^{2+} content is of paramount importance to the magnetic anisotropy, the permeability, electrical resistivity, energy losses, etc. The $Fe^{2+} - Fe^{3+}$ balance depends on the concentration of oxygen ions in the spinel structure, and because this depends on the oxygen equilibrium between the ferrite and the surrounding atmosphere during firing, atmosphere is determining for *the* $Fe^{2+} - Fe^{3+}$ *balance*. Thus a well-controlled oxygen partial pressure P_{O_2}, eg, in an N_2 atmosphere, is required. In order to obtain a desired Fe^{2+} content during cooling, P_{O_2} has to be adapted in such a way that $\log P_{O_2}$ varies linearly with $1/T$ (90,91). This may lead to P_{O_2} values as low as 0.01–0.001% at 1000–900°C, requiring very strict technical precautions. Below these temperatures, diffusion rates in the ferrites become sufficiently low to make the atmosphere less critical.

Actual temperature and atmosphere curves depend markedly on the material properties to be realized. High permeability ferrites, eg, require a microstructure with large (eg, 10–40 μm) grains without internal pores that could act as pinning points for magnetic domain walls and thus reduce permeability. This microstructure can be realized by using pure raw materials, applying intensive milling after prefiring, establishing relatively slow grain growth to ensure that the nonsoluble constituents present are transported to grain boundaries, and applying a high (up to 1400°C) top temperature for several hours. The drawback of a high sintering temperature, however, is that considerable Zn evaporation occurs. A way to handle this is to provide a high P_{O_2} at the top temperature,

then decreasing the P_{O_2} during cooling to correct the oxygen content of the ferrite.

High frequency power ferrites require small (up to a few μm) grains having electrically insulating grain boundaries. Small grains can be realized by less reactive milling after prefiring or by applying a sintering curve that has a relatively low top temperature during not too long a time. The cooling part of the firing curve has to be slow enough to facilitate segregation of additives to grain boundaries in order to provide for electrical insulation.

In general there is a great degree of interaction among the various processing steps for MnZn-ferrites. Optimization cannot concentrate on a single process step but always an integral approach of the entire process is needed, taking into account also the material under processing and its requirements on magnetic performance (92,93).

4.2. M-Type Ferrites. There are a variety of processing routes (31,33) for the four main classes of M-ferrite magnets: (*1*) sintered, (*2*) plastic bonded, (*3*) anisotropic, and (*4*) isotropic. Discussion herein is limited to the manufacture of high grade anisotropic (nonsubstituted) SrM (31). As raw materials, dry powders of strontium carbonate [1633-05-2], $SrCO_3$, Fe_2O_3, and additives such as silica [7631-86-9], SiO_2, and boric trioxide [1303-86-2], B_2O_3, are employed. The desired quantities, eg, mole ratio $Fe_2O_3/SrO \simeq 5.5$, are weighed and dry-mixed in a Müller-type mixer. The mixture is granulated in a disk agglomerator to granules of $\sim$5 mm and subsequently prefired at about 1250°C in air, by using a rotary kiln. During prefiring the raw materials react to form the desired compound, $SrFe_{12}O_{19}$. The strongly anisotropic crystal structure induces a tendency to lateral grain growth, resulting in platelet shaped crystals. The hard prefired granules are wet-milled in steel-ball mills to a fine powder. The resulting thick suspension or slurry is processed to an aligned pressed product by wet-pressing or pressure filtration in a magnetic field. During this complicated operation aligning of the crystallites, removal of water, and shaping to the desired product is performed (94). After drying, the compacts are sintered at $\sim$1250°C in air by using electrical or gas-fired furnaces. During sintering anisotropic shrinkage occurs, $\simeq$15% perpendicular and $\simeq$30% parallel to the preferred direction. Accurate dimensional control is not possible. For that reason, grinding, at least of the two pole faces, is necessary.

The most important microstructural demands are high aligning degree, high density, and small grain size with minimum platelet shape.These impose demands on the sintering process and the preceding operations. During sintering considerable densification must be realized without allowing significant grain growth. These more or less contradictory demands are fairly well realized by using sinter additives such as SiO_2 (95) or B_2O_3 and SiO_2 (96). The effect of SiO_2 has been investigated extensively. When added in the right quantity, SiO_2 and the excess SrO form a temporary liquid phase that promotes shrinkage while grain growth is suppressed. The latter is related to the dissolving of SiO_2 in the M lattice, giving rise to reaction induced grain growth inhibition (95). Important demands for the pressed products are high and homogeneous pressed density and high degree of aligning. The powder particles in the milling slurry have to be single-crystalline and free-movable in view of the aligning process, and sufficiently small in view of the sintering process. To enable a good milling perfor-

mance, the grain size in the prefired granule must not be too large. In addition, the conversion to SrM must be sufficient, otherwise a high B_r is no longer attainable. Calcination with sufficient conversion and controlled grain size can be realized in two ways (*1*) nonstoichiometric (Sr-excess) basic composition with SiO_2 and B_2O_3 addition (97), and (*2*) stoichiometric basic composition. In the former case, there is some liquid second phase during calcination that promotes the conversion and, hence, compensates for poor mixing.

Since the 1960s, the performance of M-ferrite manufacturing has improved continuously, while the price has decreased considerably. Decisive progress in quality was obtained by the application of sinter additives (98), the introduction of pressing in a magnetic field (23), and the use of Sr instead of Ba, in combination with a sophisticated application of SiO_2 (99,100). Important contributions to price reduction came from the development of multiple-die pressing and the introduction of cheap raw materials (97). In spite of the latter, the performance, in particular H_{cJ}, could be improved by a better control of prefiring, milling and sintering. In the 1970s the basis was led for the high grade technology. Different grades, varying in performance level (IP) and B_r/H_{cJ} ratio could be produced. The performance level was adjusted by the milled particle size. Limited variations in B_r/H_{cJ} ratio were realized by changes in the second phase composition and/or in the sintering temperature. More important B_r/H_{cJ} variations were realized by an Al_2O_3 or Cr_2O_3 addition. This technology, in particular the milling technique, was further refined in the next twenty years, until a "saturation" was attained around IP = 550 mT , where further decrease of the milled particle size was no longer economically feasible. In the late 1990s, a new generation of high performance ferrite magnets came to the stage (73–75): LaCo subtituted SrM ($SrLa^{3+}{}_xFe_{12-x}Me^{2+}{}_xO_{19}$ with $Me = Co^{2+}/Fe^{2+}$ and $x \sim 0.2$). This new material shows 25% increased H_{cJ} and 40% decreased TC(H_{cJ}), while B_r remains unaffected, thus realizing a real breakthrough of the performance. The improved H_{cJ} and TC(H_{cJ}) stems from an increased H_A (78–80).

5. Uses

The number of applications of spinel ferrites is very large and growing. Table 5 gives a schematic impression of the main application areas and functions (101,102). In radio, television, and measuring equipment ferrite cores are extensively applied as inductors in LC-filters. In telecommunication ferrites serve the same purpose, but have clearly higher demands on quality factor Q and temperature-plus-time stability of the inductor. High Q-values require a ferrite core having low energy losses, tan δ/μ_i, at small signals in the relevant frequency ranges, and the temperature factor $\alpha_F = (\Delta\mu_i/(\Delta T)/\mu^2{}_i$, derived from the slope of the $\mu_i(T)$ curve, has to be within very narrow limits. Because the inductance L is proportional to μ_i, this also determines the temperature dependence of L, which has to be such that it compensates for the temperature drift of the capacitor in the filter. The inductance of a coil in a circuit can be fine-tuned by bridging the gap between two ferrite core halves with an inserted ferrite adjuster. If a ferrite experiences some kind of magnetic, thermal, or mechanical disturbance, the initial permeability is instantaneously increased to an unstable value as a result

Table 5. **Applications and Functions of Spinel Ferrites**[a]

Function	Market segment									
	Measurement and control	Car electronics	Telecom-munication	Electronic data processing	Consumer electronics	Power conversion	Lighting	Household appliances	Electric tools	EMC equipment and services
coils										
tuning	X	X	X		X					
filter	X		X							
deflection				X	X					
proximity switches	X	X								
delay lines	X	X		X	X					
EMI filters	X	X	X	X	X	X	X	X	X	X
EMI cores and inductors	X	X	X	X	X	X	X	X	X	X
absorbing surfaces	X	X	X	X						X
transformers										
wideband	X	X	X	X	X					X
power		X	X	X	X	X	X	X		
line output				X	X					
LCD backlight		X	X	X	X					
current	X	X	X	X	X	X	X	X		
driver	X	X	X	X	X	X	X	X	X	
rotating					X					
output chokes		X	X	X	X	X	X	X		
magnetic regulators			X	X	X	X		X		
magnetic heads		X	X	X	X					

[a] See Ref. 101.

of a changed configuration of magnetic domain walls. From that point it returns to its original level by relatively slow diffusion processes, often associated with preferred distribution of Fe^{2+} ions or cation vacancies in the spinel structure (103,104). Filter Applications require high stability, expressed by a small disaccomodation factor $D_F = \Delta\mu_i/(\mu_i \log 10 t_2/t_1)$, describing the relative change of μ_i during a time interval (t_1,t_2) after a disturbance. Table 6 presents some specifications for typical filter ferrite grades. Stability can, among other things, be promoted by substituting stabilizers, eg, Ti^{4+} or Sn^{4+}, into the ferrites (105).

As electronic equipment is increasingly used electromagnetic compatibility (EMC) has become an issue of fast-growing importance (see ELECTRONIC MATERIALS). Emission of unwanted signals has to be limited, as does the sensitivity of equipment to incoming interferences. These signals are subjected to international and national regulations. For both purposes, ferrites are being increasingly used because ferrites can supply electromagnetic interference (EMI) suppression as inductor cores in low pass LC-filters, as well as serve as selective impedance inductors in series with circuit load impedances, without the use of capacitors.

The objective is to block unwanted signals having frequencies that differ sufficiently from those of wanted signals, which should pass with virtually no attenuation. Effective blocking is obtained in case of high impedances $Z = 2\pi fL$. Because L is proportional to $(\mu'^2 + \mu^2)^{1/2}$ and because this expression as a function of f shows a resonant maximum in a frequency region depending on the ferrite's chemical composition and microstructure, the choice of the ferrite grade is determined by the frequency to be blocked. In filters for frequencies below ~500 kHz, high permeability 3E-materials, which according to Table 6 are primarily intended for wide-band transformer applications, are often used; between 500 kHz and a few MHz ferrites the 3C90/94/96 and 3F grades, meant in the first instance as power materials, offer effective solutions. Above a few MHz the Ferroxcube NiZn grades 4A15 and 4C65 at >3 MHz and >30 MHz, respectively, become important as high frequency filter materials, and grades 3S1 and 4S2, up to 30 MHz and from 10 to 1000 MHz, respectively, are used as suppressors without using separate capacitors.

In communication systems and modern digital networks, signal and pulse transformers known as wide-band transformers are used. The functions are to transform signal amplitudes and to provide impedance matching and dc isolation, usually at low signal power levels. Good wide-band characteristics for analogue signals or digital pulses requires a optimum coupling between the transformer windings, and high inductances in the case of pulse transformers. Well-known high grade materials other than those given in Table 6 are the Epcos T30 series (106) and the TDK H5 series (107). All these high permeability ferrites are used in closed cores, such as ring cores, or composed cores having carefully polished contact surfaces.

Recent digital transmission systems, denoted as DSL systems, make use of wide-band transformers with more severe requirements on low signal distortion. For this purpose new ferrites have been developed with an improved lineairy of the BH loop resulting in a lower total harmonic distortion (108–110).

Another area having a wide range of applications for modern ferrites is power conversion such as switched mode power supplies (SMPS) (111) and

Table 6. **Properties of MnZn and NiZn Ferrite Grades**[a]

A. Materials and applications[b]

Property	Test conditions				Filter inductors			Wideband transformers[c]						
Symbol	f(kHz)	B_{peak} or H	T(°C)	unit	3D3	3H3	3B7	3E27	3E28	3E5	3E55	3E6[c]	3E7[c]	3E8[c]
$\mu_1(\pm 20\%)$	≤10	≤mT	25		750	2000	2300	6000	400	10,000	10,000	12,000	15,000	18,000
$\tan\delta/\mu_1$	10	≤0.1 mT	25	$(\times 10^{-6})$							≤10	≤10	≤10	≤10
	30					≤1.6				≤25	≤30	≤30	≤30	≤30
	100					≤2.5	≤5	≤15	≤5	≤75				
	300				≤10									
	500						∼25							
	1000				≤30		∼120							
	3000													
	10000													
η_B	10	1.5–3 mT	25	$10^{-3}T^1$						≤1	≤0.2	≤1	≤1	≤1
	100				≤1.8	≤0.6								
α_F	≤10	≤0.1 mT	5–25	$10^{-6}K^{-1}$		0.7 ± 0.3								
			25–55			0.7 ± 0.3								
			25–70		1.5 ± 1	0.7 ± 0.3	0 ± 0.6							
D_F	10	≤0.1 mT	25	$(\times 10^{-6})$	≤12	≤3	≤3.5							
	100													
B	10	250 A/m	100	mT	∼260	∼250	∼300	∼250	∼260	∼210	∼200[d]	∼210	∼210	∼150
		3000 A/m	25		∼400	∼400	∼450	∼400	∼400	∼380	∼380	∼380	∼380	∼380
H_c	10		25	A/m	∼75	∼15	∼15	∼5	∼5	∼5	∼5	∼4	∼4	∼4
B_r	10		25	mT	∼150	∼70	∼150	∼100	∼100	∼80	∼150	∼100	∼100	∼100
T_c				°C	≥200	≥160	≥170	≥150	≥145	≥125	≥100	≥130	≥130	≥100
p	DC			Ωm	∼2	∼2	∼1	∼0.5	∼1	∼0.5	∼0.1	∼0.1	∼0.1	0.1
density				kg/m^3	∼4700	∼4700	∼4800	∼4800	∼4800	∼4900	∼5000	∼4900	∼4900	∼5000
ferrite type					MnZn	MnZn	MnZn	MnZn	MnZn	MnZn	MnZn	MnZn	MnZn	MnZn

B. Materials and applications for EMI-suppression[e]

Property	Test conditions				EMI-suppression												
Symbol	f(kHz)	B_{peak} or H	T(°C)	unit	3B1	3C11	3E5	3E6[f]	3E7[f]	3E8[f]	3E25	3E26	3E27	4A11	4A15	4B1	4C65
μ_i(±20%)	≤10		25		900	4300	10,000	12,000	15,000	18,000	6,000	7,000	6,000	850	1200	250	125
tanδ/μ_i	30	≤0.1 mT	25	($\times 10^{-6}$)			≤25	≤30	≤30	≤30							
	100					≤20	≤75				≤25	≤20	≤15				
	300					≤200					≤200						
	450				≤50												
	1,000													≤100	≤300	≤90	
	3,000													≤1000	≤1500	≤300	≤80
	10,000																≤130
B	10	250 A/m	100	mT	∼200	∼180	∼210	∼210	∼210	∼200	∼180	∼290	∼280	∼180	∼180	∼260	∼250
		3000 A/m	25		∼370	∼340	∼380	∼380	∼380	∼380	∼380	∼450	400	∼320	∼340	∼350	∼380
H_c			25	A/m	∼25	∼10	∼5	∼4	∼4	∼4	∼5	∼5	∼5	∼35	∼25	∼150	∼250
B_r				mT	∼190	∼120	∼80	∼100	∼100	∼100	∼100	∼120	∼120	∼110	∼150	∼240	∼280
T_c				°C	≥150	≥125	≥125	≥130	≥130	≥100	≥125	≥155	≥150	≥125	≥125	≥250	≥350
p	DC		25	Ωm	∼0.2	∼1	∼0.5	∼0.1	∼0.1	∼0.1	∼0.5	∼0.5	∼0.5	$\sim 10^5$	$\sim 10^5$	$\sim 10^5$	$\sim 10^5$
density				kg/m^3	∼4800	∼4900	∼4900	∼4900	∼4900	∼5000	∼4900	∼4900	∼4800	∼5100	∼5100	∼4600	∼4500
ferrite type					MnZn	MnZn	MnZn	MnZn	MnZn	MnZn	MnZn	MnZn	MnZn	NiZn	NiZn	NiZn	NiZn

Table 6 (*Continued*)

C. Materials and applications for EMI-suppression[g]								
Property	Test Conditions				EMI-suppression			
Symbol	f(MHz)	B_{peak} or H	T (°C)	unit	3S1	3S3	3S4	4S2
μ_i (±20%)	≤0.01	≤0.1 mT	25		~4000	~350	~1700	~700
|Z|[h]	1	≤0.1 mT	25	Ω	≥30			
	3						≥25	
	10				≥60			
	30					≥25	≥60	≥50
	100					≥60	≥80	
	300					≥100	≥90	≥90
B	0.01	250 A/M	100	mT	~180	~250	~140	~180
		3000 A/M	25		~400	~350	~350	~350
H_c			25	A/m	~10	~60	~20	~30
B_i			25	mT	~120	~230	~170	~120
J_c				°C	≥125	≥225	≥110	≥125
p	DC			Ωm	~1	$\sim 10^4$	$\sim 10^4$	$\sim 10^5$
density				kg/m^3	~4900	~4800	~4800	~5000
ferrite type					MnZn	MnZn	MnZn	NiZn

D. Materials and applications[i]

Property	Test Conditions				Power transformers and power inductors													
Symbol	f(kHz)	$B_{peak\ or\ H}$	T(°C)	unit	3C30	3C34	3C81	3C90	3C91	3C92	3C93	3C94	3C96	3F3	3F35	3F4	4F1	3R1
μ_i (±20%)	≤10	≤0.1 mT	25		2100	2100	2700	2300	3000	1500	1800	2300	2000	2000	1400	900	~80	800
B	10	250 A/m	100	mT	≥370	≥370	~330	≥340	≥330	~410	~380	≥340	≥370	≥330	≥330	≥300	≥100	≥285
		1200 A/m	100		~440	~440	~360	~380	~370	~460	~430	~380	~440	~370	~420	~350	~300	~340
		3000 A/m	25		~500	~500	~450	~450	~450	~550	~530	~450	~500	~450	~500	~400	~350	~420
H_c	10		25	A/m	~15	~15	~15	~15	~15	~15	~15	~15	~15	~15	~40	~60	~150	~40
B_r	10		25	mT	~180	~180	~110	~170	~110	~170	~170	~170	~170	~150	~200	~150	~200	~340
P_v	25	200 mT	100	kW/m^3	≤80		≤185	≤80										
	100	100 mT			≤80	≤80		≤80	~55[j]	~50	~50	≤60	≤45	≤80				
	100	200 mT			~450	≤400		~450	~330[j]	~350	~350	≤400	≤330					
	200	100 mT				~170												
	400	50 mT										≤170	≤140	≤150	≤80			
	500	50 mT									~300				≤120			
		100 mT													~800			
	1000	30 mT														≤200		
		50 mT																
		70 mT																
	3000	10 mT														≤320	≤200	
		30 mT																
	10,000	5 mT															≤200	
T_c				°C	≥240	≥240	≥210	≥220	≥220	≥280	≥240	≥220	≥240	≥200	≥240	≥220	≥260	≥230
p	DC			Ωm	~2	~5	~1	~5	~5	~5	~5	~5	~5	~2	~10	~10	~10^5	~10^3
density				kg/m^3	~4800	~4800	~4800	~4800	~4800	~4800	~4800	~4800	~4800	~4750	~4750	~4700	~4600	~4700
ferrite type					MnZn	MnZn	MnZn	MnZn	MnZn	MnZn	MnZn	MnZn	MnZn	MnZn	MnZn	MnZn	NiZn	MnZn

[a] see Ref. 101.
[b] Properties measured on sintered, unground ring cores of dimensions Ø25 × Ø15 × 10 mm, which are not subjected to external stresses.
[c] Measured on sintered, unground ring cores of dimensions Ø14 × Ø9 × 5 mm, which are not subjected to external stresses.
[d] At 80°C.
[e] Properties measured on sintered, unground ring cores of dimensions Ø25 × Ø15 × 10 mm, which are not subjected to external stresses.
[f] Measured on sintered, unground ring cores of dimensions Ø14 × Ø9 × 5 mm, which are not subjected to external stresses.
[g] Properties measured on sintered, unground ring cores of dimensions Ø25 × Ø 15 × 10 mm, which are not subjected to external stresses.
[h] Measured on a bead of dimensions Ø5 × Ø2 × 10 mm.
[i] Properties measured on sintered, unground ring cores of dimensions Ø25 × Ø15 × 10 mm, which are not subjected to external stresses.
[j] At 60 °C.

LCD backlight inverters (112). SMPS devices are used for ac–dc conversion and for ac–dc transformation. An incoming ac voltage is first rectified and filtered and then chopped by a high frequency switch. The chopped signals are transformed to the desired voltage levels, rectified, and filtered to provide the required dc output. The result is measured by a control unit, which, in case of deviations, supplies corrective signals to the switching circuit. For the heart of the operation, the voltage conversion, several circuit designs are in use, making extensive use of ferrites as transformer core materials (111). Besides this, ferrites are used in SMPS as input filters and output chokes. Transformer ferrites must show low energy losses at high induction levels at higher and higher frequencies (52–55,113,114). The latter facilitates reduction of volume and weight of the SMPS devices.

Achieving, eg, a decrease in energy loss level in an upgraded ferrite of 25 % may result in a reduction of volume of the core shape with >20 %. For this purpose highly efficient core shapes and winding configurations have also been developed (113–116). The decrease in weight of power supplies is illustrated in Figure 8.

Ferrites allowing for operation at frequencies well above 1 MHz have also become available, eg, 3F4 and 4F1 (Table 6). Other newer industrial power ferrites are the Epcos N-series (29,106) the TDK PC series (29,106), and the AVX/Thomson B-series (29,117). While moving to higher frequencies, the ferrites have been optimized for different loss contributions, eg, hysteresis losses, eddy current losses, and resonance losses. Loss levels are commonly specified at 100°C because ambient temperature in most power applications is ∼60°C plus an increase caused by internal heat dissipation of ∼40°C. In some areas, like in automotive and lighting applications higher operating temperatures can be applicable. For this purpose special ferrites are designed with a specification of loss levels at 140°C (118). An important property for ferrites used in power inductors (output chokes) is a high flux saturation level to achieve a high inductance stability for bias currents (119,120).

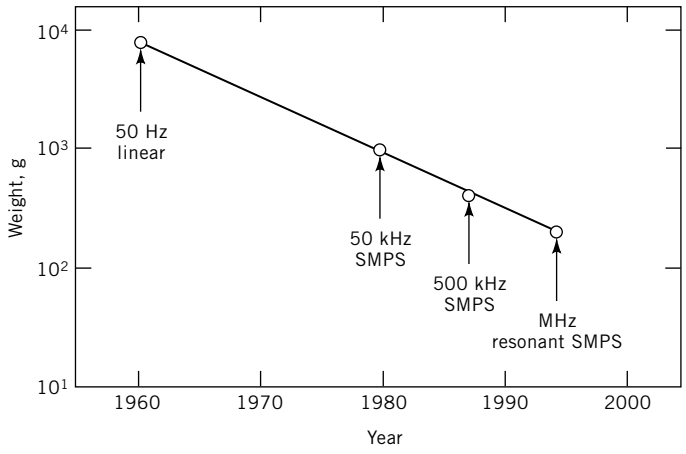

Fig. 8. SMPS = switch mode power supply. Weight reduction of 100-W power supplies from the 1960s through the early 1990s.

Table 7. **Permanent Magnet Materials (high grade values)**[a]

Parameter	Ferrite[b]	NdFeB	SmCo	Alnico-9
B_r, mT	145	1200	900	1000
H_{cJ}, kA/m	270	> 1000	1200	100
$(BH)_{max}$[c] kJ/m^3	34	280	150	40
B/μ_0H at $(BH)_{max}$	1.0	1.0	1.0	20
density, kg/m^3	4900	7400	8300	7300
P, Ω m	10^4	10^{-6}	5×10^{-7}	5×10^{-7}
T_c, K	750	585	995	860
$\alpha(B_r)$, % K^{-1}	−0.2	−0.13	−0.05	−0.02
$\alpha(H_c)$, % K^{-1}	$+0.4^{\alpha}$	−0.6	−0.3	−0.03
price per ratio per unit[d]				
-weight	1	30	40–50	5
-magnetic energy[e](20°C)	1	5.9	11–16	2.9
-motor performance[f] (100°C)	1	4.2	6.7	6.9
world production 1999[g]				
$t \times 10^3$ (estimates)	450	9	1	10
$\$ \times 10^6$	2700	1450	250	300

[a] Refs. 24,121.
[b] For unsubstituted ferrite.
[c] To convert joules to calories, divide by 4.184.
[d] Ferrite is taken as reference.
[e] Price per unit magnetic energy = price per unit weight × density/$(BH)_{max}$.
[f] As d, but $(BH)_{max}$ is replaced by Br*H_g, were H_g is the max. reverse field in a motor (121).
[g] Total production, bonded magnets included (24).

5.1. M-Type Ferrites. Since their introduction on the market in the early 1950s, M-ferrites have gradually acquired a dominant position in the permanent magnet market (Table 7), mainly by replacing the established alnico magnets in many applications. The growth rate has always been ∼10% year. The most important feature behind the great economic success of ferrite magnets is the low price per unit of available magnetic energy, attributable to the relatively low cost and wide availability of the raw materials. In the past 20 years, however, dominance of ferrites in terms of market value has begun to decrease because of the growing importance of rare-earth-based metallic magnet material (see LANTHANIDES). This material, $Nd_2Fe_{14}B$, has largely extended the separate market of low volume, high price, high performance magnets for miniaturized systems, which had been represented only by the very expensive SmCo-based magnets.

A large variety of M-ferrite magnets and applications is available. Table 8 gives a survey of typical commercial grades. Bonding of the microscopic crystallites to solid bodies is performed either by sintering or by plastic bonding. The latter produces a plasto-ferrite. In both cases, the crystallites may be either randomly oriented (isotropic) or aligned with the c axis in one direction (anisotropic). Depending on the binder used, plasto-ferrites may be flexible or rigid. Special advantages of sintered materials are high magnetic quality, close dimensional control when machined, and relatively high mechanical strength. When these properties are not of prime importance, plasto-ferrites may be preferred because

Table 8. **Properties of Commercial M-Ferrites**[a]

Type	M[b]	B_r mT	H_{cB}, kA/m	H_{cJ}, kA/m	$(BH)_{max}$,[d] kJ/m^3	μ_{rec}[e]	H_{sat},[f] kA/m	$\alpha(B_r)$,[g] %/K	$\alpha(H_{cJ})$,[g] %/K	ρ,Ω m	Density, kg/m^3	Typical application	Market share, %
						Sintered							
isotropic	Ba	220	135	220	7.5	1.2	800	−0.2	+0.4	10^4	4900	rotors for cycle generators	∼15
anisotropic													
low H_c	Ba	400	160	165	29	1.1	550	−0.2	+0.4	10^4	5000	flat rings for loudspeakers	
medium H_{cJ}	Sr	370	245	255	25	1.1	770	−0.2	+0.4	10^4	4900	segments for auxiliary	
		410	270	280	32	1.05	840				4990		
high H_{cJ}	Sr	390	290	330	29	1.1	1000	−0.2	+0.4	10^4	4930	automotive motors	∼55
		370	274	360	25	1.1	1100		+0.4		4920		
high quality[h]	*SrLa*	*420*	*333*	*360*	*33*	*1.05*	*1100*		+0.25		*5000*		
very high H_{cJ}	Sr	365	280	405	24	1.1	1200	−0.2	+0.4	10^4	5000	segments for starter motors	
high quality[h]	*SrLa*	*405*	*318*	*400*	*31*	*1.05*	*1200*		+0.25		*5000*		
						Plastic bonded							
flexible isotropic	Ba	125	88	190	2.8	1.15	800	−0.2	+0.4	10^7	3100	doorcatches (refrigerators)	
		145	96	190	3.6	1.15	800	−0.2	+0.4		3700	small dc motors	∼15
anisotropic	Sr	200	140	200	8.0	1.05		−0.2	+0.4	10^8	3500	(pumps for washing machines)	
		250	176	240	12.0	1.05		−0.2	+0.4		3500		
rigid isotropic	Ba	80	58	190	0.9	1.15	800	−0.2	+0.4	10^8	2500	correction magnets for TV	
		155	104	190	4.4	1.15	800	−0.2	+0.4	10^4	3900		∼15
anisotropic	Sr	245	100	260	12.0	1.05	800	−0.2	+0.4	10^5	3500	small dc motors	
		270	196	260	14.0	1.05	800			10^5	3900	(domestic appl., car mirrors)	

[a] Refs. 122,123.
[b] Normally applied M-ferrite.
[d] To convert joules to calories, divide by 4.184.
[e] Recoil permeability.
[f] $H \geq H_{sat}$ is needed to establish maximum B_r and H_{cJ}.
[g] α = Temperature coefficient (0.8 kA/m · K for BaM and 0.95 kA/m.K for unsubstituted SrM).
[h] LaCo-substituted.

of lower price or special mechanical properties and shaping possibilities. Anisotropic materials are applied when high magnetic quality is essential. The less expensive isotropic material is preferred when low magnetic quality is acceptable or when the properties have to be isotropic.

The anisotropic sintered form is by far the most important one. It is produced in various grades that can be classified according to the coercivity level, which determines te application. The first group with lowest coercivity is used for loudspeakers, where a high B_r is essential, whereas a relatively low H_{cJ} is acceptable. The other groups are used for different types of motors, requiring quite distinct H_{cJ} levels. In these cases a high B_r is also desired, but in fact it is limited by the performance level (IP) of the used material. The performance level may vary around 50 units within one coercivity group. Figure 9 shows typical demagnetization curves for the materials of Table 8 (122,123).

Prices for the different material groups are largely influenced by product size and shape and the quantity of production. Apart from product shape, the main price-determining factor is the performance level (IP).

Prices for the powder and the sintered product, are roughly on the order of \$1 and \$3–6, respectively.

A variety of shapes and sizes exists for the commercial M-magnets. Most M-ferrite products are flat owing to the relatively high H_c and moderate B_r. Basic shape groups are rings, disks, plates, rods, cylinders, blocks, strips, and segments. Each shape group in turn contains a number of products. The more complicated forms are preferably made from rigid plasto-ferrite because of versatility in shaping without the necessity of finishing.

Products, whether or not anisotropic, may have different magnetization modes. That is, magnetization may be from one side to the opposite one, or along one side (lateral magnetization). The resulting polar surfaces may contain regions having opposite polarity (poles), separated by a neutral zone. Different pole numbers and configurations are possible. Combinations of these possibilities give rise to a variety of magnetization modes. All products may be anisotropic and products of the same appearance may have a different aligning mode.

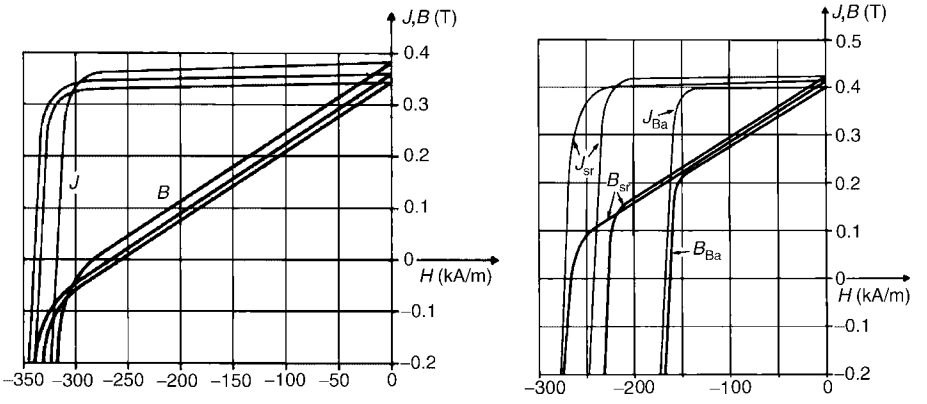

Fig. 9. Demagnetization curves for M-ferrites at high K values (see Table 8).

The most important aligning modes are shown in Figure 10. When a complex magnetization mode is desired, isotropic materials are preferred. Lateral magnetization, always in multipole, is only applied to isotropic materials.

As compared to the classical alnico-magnets, M-ferrite magnets have some distinct advantages. These are relatively high H_c, high resistivity, low price, low density, high chemical resistance, and the suitability of being applied as (flexible) plastoferrite. The relatively high H_c and, in particular, the low price have contributed to economic success.

The most important disadvantages are moderate B_r and $(BH)_{max}$, relatively high temperature coefficients αB_r and αH_c, and poor mechanical properties (low strength, brittleness). The moderate B_r and $(BH)_{max}$ are perhaps the less serious, since it may be compensated by an increased cross-sectional area. However, the latter two disadvantages exclude certain applications where the magnet is exposed to strong mechanical stresses or impacts, or where the surrounding temperature temporarily drops far below the normal operating temperature. In the latter case the H_c may temporarily decrease so far that the knee in the BH curve is surpassed, resulting in a partial irreversible demagnetization of the magnet.

Owing to low price, M-ferrites have replaced other magnet materials in existing systems, whether or not modification has been made to the system. This is particularly so in static applications where small demagnetizing fields are involved. A typical example is the application of flat M-ferrite rings used instead of the high metallic center-core magnets in loudspeaker systems. The high H_c has stimulated the development of new systems. This applies especially

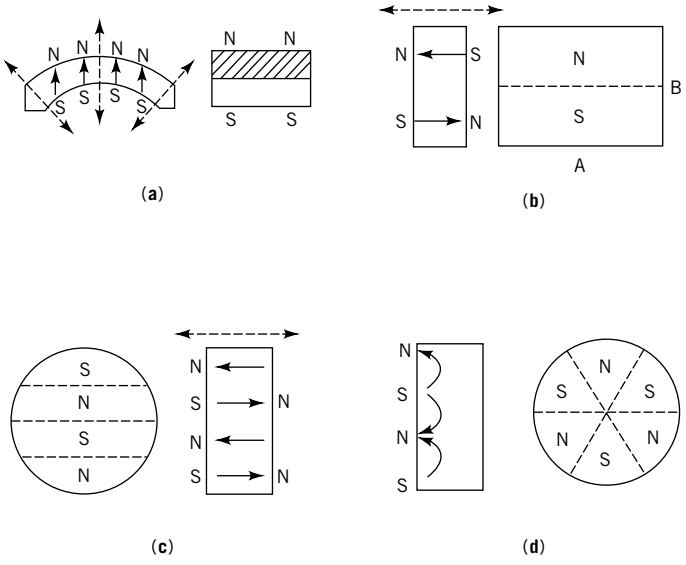

Fig. 10. Aligning-magnetizing modes where (←- - →) represents aligning direction and (—) the neutral zones. (**a**) Segment, radially aligned, diametrically magnetized; (**b**) block, perpendicularly aligned and magnetized, two poles, neutral zone parallel to A; (**c**) disk, axially aligned and magnetized, four poles, neutral zone diametrical; and (**d**) disk, isotropic, laterally magnetized, six poles, where the neutral zone is radial.

Table 9. **Applications of M-Ferrites**

Magnet type	Market sector,	Examples
motor-segments (arcs)	automotive	dc motors in cars; windshield wipers, starter, ABS system
	domestic	synchronous motors, kitchen appliances, rechargeable tools
	industrial	servomotors, machine tools
loudspeaker rings	audio-car	car radio
	hifi	music centers, speaker systems
	portable video-television	portable radio
miscellaneous (blocks, etc)	industrial	separators, couplings, industrial motors
	domestic	sticking devices, cycle dynamos
	others	small motors for audio / video, toys

to dynamic applications where periodically high demagnetizing fields are involved. A typical example is the electromotor, which has strong demagnetizing fields. Electromotors are being developed requiring very high H_{cJ} values which lie far outside the scope of the alnico materials (131), eg, the starter motor, requiring $H_{cJ} > 350$ kA/m.

Table 9 gives a survey of the most important applications of sintered *M*-ferrite magnets. The main products which together form ~50% of the total production are anisotropic segments for dc motors in cars and anisotropic rings for loudspeakers . Large scale production is concentrated on systems requiring relatively large magnets, thus taking greatest advantage of low material price.

BIBLIOGRAPHY

"Ferrites" in *ECT* 2nd ed., Vol. 8, pp. 881–901, by G. Economos, Allen-Bradley Co.; in *ECT* 3rd ed., Vol. 9, pp. 881–902, by T. G. Reynolds III, Ferroxcube Corp; in *ECT* 4th ed., Vol. 10, pp. 381–413, by F. X. N. M. Kools and D. Stoppels, Philips Components; "Ferrites" in *ECT* (online), posting date: December 4, 2000, by F. X. N. M. Kools, D. Stoppels, Philips Components.

CITED PUBLICATIONS

1. W. L. Bragg, *Philos. Mag.* **30**, 305 (1915).
2. G. Aminoff, *Geol. Fören. Förhandl.* **47**, 283 (1925).
3. J. L. Snoek, *New Developments in Ferromagnetic Materials*, Elsevier, Amsterdam, The Netherlands, 1947.
4. J. Smit and H. P. J. Wijn, *Ferrites*, Philips' Technical Library, Eindhoven, The Netherlands, 1959.
5. J. L. Snoek, *Physica* **3**, 463 (1936).
6. T. Takei, *J. Electrochem. Jpn.* **5**, 411 (1937).

7. L. Néel, *Ann. Phys.* **3**, 137 (1948).
8. M. Takano, N. Nakanishi, Y. Takeda, and T. Shinjo, in H. Watanabe, S. Iida, and M. Sugimoto, eds., *Ferrites*, Proceedings of the 3rd International Conference on Ferrites (ICF-3), Center for Academic Publishing Japan, Tokyo, 1981, p. 389.
9. M. M. Abou-Sekkina, *Adv. Ceramics* **15**, 553 (1985).
10. A. H. Bobeck and E. Della Torre, *Magnetic Bubbles*, North Holland Publishing Co., Amsterdam, The Netherlands, 1979.
11. M. A. Gilleo, in E. P. Wohlfarth, ed., *Ferromagnetic Materials*, Vol. 2, North-Holland Publishing Co., Amsterdam, The Netherlands, 1982, Chapt. 1.
12. P. Hansen and J. P. Krumme, *Thin Solid Films* **114**, 69 (1984).
13. S. L. Blank and co-workers, *J. Appl. Phys.* **50** 2155 (1979).
14. J. J. Went and E. W. Gorter, *Philips Techn. Rev.* **13**, 181 (1951–1952).
15. M. Sugimoto, in Ref. 11, Vol. 3, Chapt. 6.
16. G. H. Jonker, H. P. J. Wijn, and P. B. Braun, *Philips Techn. Rev.* **18**, 145 (1956/57).
17. Y. H. Chang, C. C. Wang, T. S. Chin, and F. S. Yen, *J. Magn. Magn. Mats.* **72**, 343 (1988).
18. R. L. Harvey, I. Gordon, and R. A. Braden, *RCA Rev.* **22**, 648 (1961).
19. G. Winkler and H. Dösch, *Proceedings of the 9th European Microwave Conference*, Microwave Exhibitions and Publications, Sevenoaks, UK, 1979, p. 13.
20. M. P. Sharrock, *IEEE Trans. Magn.* MAG25, 4374 (1989).
21. M. Noda, Y. Okazaki, K. Hara, and K. Ogisu, *IEEE Trans. Magn.* MAG26, 81 (1990).
22. J. J. Went, G. W. Rathenau, E. W. Gorter, and G. W. van Oosterhout, *Philips Techn. Rev.* **13**(7), 194 (1952).
23. A. L. Stuyts, G. W. Rathenau, and G. H. Weber, *Philips Techn. Rev.* **16**(5/6), 141 (1954).
24. "Permanent Magnets", Eur. Powd. Metall. Association, 2001, p. 17.
25. A. Broese van Groenou, P. F. Bongers, and A. L. Stuyts, *Mater. Sci. Eng.* **3**, 317–392 (1968–1969).
26. J. Nicolas, in Ref. 11, Vol. 2, Chapt. 2.
27. P. I. Slick, in Ref. 11, Vol. 2, Chapt. 3.
28. S. Krupicka and P. Novak, in Ref. 11, Vol. 3, Chapt. 4.
29. E. C. Snelling, *Soft Ferrites*, 2nd ed., Butterworth & Co. Publishers Ltd., Kent, UK, 1988.
30. A. Goldman, *Modern Ferrite Technology*, Van Nostrand Reinhold Co., Inc., New York, 1990.
31. C. A. M. van den Broek, and A. L. Stuyts, *Philips Techn. Rev.* **37**(7), 157 (1977).
32. H. Kojima, in Ref. 11, Vol. 3, Chapt. 5.
33. H. Stäblein, in Ref. 11, Vol. 3, Chapt. 7.
34. S. Chikazumi, *Physics of Magnetism*, John Wiley & Sons, Inc., New York, 1978.
35. K. Ohta, *J. Phys. Soc. Jpn.* **18**, 685 (1963).
36. D. Stoppels, *J. Appl. Phys.* **51**, 2789 (1980).
37. E. Röss, I. Hanke, and E. Moser, *Z. Angew. Phy.* **17**, 504 (1964).
38. D. J. Perduijn and H. P. Peloschek, *Proc. Br. Cer. Soc.* **10**, 263 (1968).
39. E. G. Visser, M. T. Johnson and P. J. van der Zaag, *Proceedings of the 6th International Conference on Ferrites (ICF-6)*, The Japanese Society of Powder and Powder Metallurgy, Tokyo, 1992.
40. K. Ohta and N. Kobayashi, *Jpn. J. Appl. Phys.* **3**, 576 (1964).
41. E. Röss and E. Moser, *Z. Angew. Phys.* **13**, 247 (1961).
42. T. Iimura, T. Shinohara, and M. Kudo, in Ref. 8, 1981, p. 726.
43. D. Stoppels, P. G. T. Boonen, J. P. M. Damen, L. A. H. van Hoof, and K. Prijs, *J. Magn. Magn. Mats.* **37**, 123 (1983).
44. J. C. Slonczewski, *J. Appl. Phys.* **32**, 253 S (1962).

45. J. G. M. de Lau, *Philips Res. Repts. Suppl.* **6**, 45 (1975).
46. M. T. Johnson, *Proceedings of the 5th International Conference on Ferrites (ICF-5)*, C. M. Srivastava and M. J. Patni, eds. Oxford and IBH Publishing Co. PVT., Ltd., New Delhi, 1989, p. 605.
47. T. G. W. Stijntjes, J. Klerk, and A. Broese van Groenou, *Philips Res. Rep.* **25**, 95 (1970).
48. T. Akashi, *Trans. Jpn. Inst. Met.* **2**, 171 (1961).
49. T. Akashi, *NEC Res. Dev.* **8**, 89 (1966).
50. U. Wagner, *J. Magn. Magn. Mats.* **4**, 116 (1977).
51. A. D. Giles and F. F. Westendorp, *J. Phys. Colloq. Suppl.* **38**, C1-317 (1977).
52. T. G. W. Stijntjes and J. J. Roelofsma in F. F. Y. Wang, ed., *Proceedings of the 4th International Conference on Ferrites (ICF-4), Pt. II*, San Francisco, 1985, p. 493.
53. T. G. W. Stijntjes in Ref. 45, 1989, p. 587.
54. E. G. Visser, J. J. Roelofsma, and G. J. M. Aaftink in Ref. 45, 1989, p. 605.
55. T. Sano, A. Morita, and A. Matsukawa, *Power Electronics PCIM* 19 (July 1988) and Ref. 45, 1989, p. 595.
56. K. Ishino and Y. Narumiya, *Am. Cer. Bull.* **66**, 1469 (1987).
57. M. H. Berger, J. Y. Laval, F. Kools, and J. Roelofsma in Ref. 45, 1989, p. 619.
58. J. W. Waanders, *Data Handbook of Soft Ferrites*, Philips Components, Eindhoven, The Netherlands, 1993.
59. J. L. Snoek, *Physica* **14**, 207 (1948).
60. V. Aldelsköld, *Ark. Kemi, Min. Geol.* **12A**(29), 1 (1938).
61. P. Braun, *Philips Res. Rept.* **12**, 491 (1957).
62. W. D. Townes, J. H. Frang, and A. J. Perrotta, *Z. Kristallogr.* **125**, 437 (1967).
63. A. J. Mountvala and S. F. Ravitz, *J. Am. Cer. Soc.* **45**(6), 285 (1962).
64. B. T. Shirk and W. R. Buessem, *J. Appl. Phys.* **40**, 1294 (1969).
65. (a) R. Pauthenet and G. Rimet, *Compt. Rend.* **249**, 656 (1959). (b) J. S. van Wieringen, *Philips Techn. Rev.* **28**, 33 (1967).
66. E. W. Gorter, *Proc. IEEE* **104B**, 255 S (1957).
67. E. F. Bertaut, A. Deschamps, R. Pauthenet, and S. Pickart, *J. Phys. Rad.* **20**, 404 (1959).
68. C. M. Fang and co-workers, to be published.
69. R. Gemperle, E. V. Shtolts and M. Zeleny, *Phys. Stat. Sol.* **3**, 2015 (1963).
70. H. Zijlstra in Ref. 11, Vol. 3, Chapt. 5.
71. F. K. Lotgering, P. R. Locher, and R. P. van Stapele, *J. Phys. Chem. Solids* **41**, 481 (1980).
72. E. C. Stoner and E. P. Wohlfarth, *Philos. Trans. R. Soc., London* **240A**, 599 (1948).
73. Taguchi and co-workers, *Proc. 8th Int. Conf. Ferrites, ICF8* (2000).
74. Kubota and co-workers, *Proc. 8th Int. Conf. Ferrites, ICF8* (2000).
75. Kools and co-workers, *Proc. 8th Int. Conf. Ferrites, ICF8* (2000).
76. G. Albanese and A. Deriu, *Ceramurgia Int.* **5**(1), 3 (1979).
77. H. R. Zai, J. Z. Liv, and M. Lu, *J. Appl. Phys.* **52**, 2323 (1981).
78. K. Iida, et al., *J. Magn. Soc. Jpn.* **23** (1999).
79. A. Morel and co-workers, *Proc. 8th Int. Conf. Ferrites, ICF8* (2000).
80. R. Grössinger, *Proc. 8th Int. Conf. Ferrites, ICF8* (2000).
81. R. Schippan and K. A. Hempel in Ref. 51, Pt II, p. 579.
82. F. Kools, *Proc. Magn. Mats. Appl. (MMA), J. Phys. (Paris)* **46**, C6-349, Grenoble (1985).
83. F. Kools in Ref. 45, p. 417.
84. H. J. H. van Heffen, *Electr. Compon. Appl.* **3**(1), 22 (1980).
85. F. Kools, *Sci. Ceramics Soc. Française Cér.* **7**, 27 (1973).

86. M. Kolenbrander, V. T. Zaspalis, R. Mauczok, A. Essing and A. Rush, "Relation between morphology and reactivity for high purity Ruthner iron oxides", *8th International Conference on Ferrites, 2Aa I-3, Kyoto, Japan*, 2000.
87. O. Kimura and A. Chiba in Ref. 51, Pt. I, p. 115.
88. V. T. Zaspalis and R. Mauczok, "Advanced Processing of MnZn-Ferrites", Philips Forschungslaboratorien GmbH, Internal Report 1364/99, 1999.
89. R. Mauczok and V. T. Zaspalis, *J. Eur. Ceram. Soc.* **20**, 2121, 2000.
90. J. M. Blank, *J. Appl. Phys. Suppl.* **32**, 378S (1961).
91. R. Morineau and M. Paulus, *IEEE Trans. Magn.*, **MAG11**, 1312 (1975).
92. V. T. Zaspalis, R. Mauczok, M. Kolenbrander and J. Boerekamp, "Low-loss MnZn ferrites through optimised processing", in *9th CimTec World Ceramics Congress* (P. Vincenzini ed.), 1999, p. 401.
93. V. T. Zaspalis, R. Mauczok, M. Kolenbrander and J. Boerekamp, *J. Phys.* **7**, C1 (1997).
94. F. Kools and O. Fiquet, in G. de With, R. A. Terpstra and R. Metselaar, eds., *Euroceramics*, Vol. 1, Elsevier Applied Science, London, 1989, p. 258.
95. F. Kools, *Sci. Sintering* **17(1)**, 49 (1985).
96. H. Harada, in Ref. 8, p. 354.
97. C. A. M. van den Broek, *Proceedings of the 3rd European Conference on Hard Magnetic Materials*, Bond Materialen Kennis, Amsterdam, The Netherlands, 1973, p. 53.
98. Fr. Pat. 1,085,491 (1954) (to N. V. Philips Gloeilampen Fabrieken).
99. A. Cochardt, *J. Appl. Phys.* **34**, 123 (1963).
100. G. S. Krijtenburg, *Proceedings of the 1st European Conference on Hard Magnetic Materials* Vienna, 1966 (unpublished).
101. E. J. Pateer, *Soft Ferrite Selection Guide*, Ferroxcube, Eindhoven, The Netherlands, 2003.
102. Data on commercial Soft Ferrite Materials (FXC grades): www.ferroxcube.com
103. A. Braginski, *Phys. Stat. Sol.* **11**, 603 (1965).
104. A. Fox, *J. Phys.* **D4**, 1239 (1971).
105. J. E. Knowles, *Philips Res. Rep.* **29**, 93 (1974).
106. J. Hess, *Siemens Components* **26**, 142 (1991).
107. H. Tsunekawa, A. Nakata, T. Kamijo, K. Okutani, R. K. Mishra, and G. Thomas, *IEEE Trans. Magn.* MAG**15**, 1855 (1979).
108. D. J. Huisman, and J. G. Boerekamp, E. G. Visser, "Core shape modifications for DSL technology", *8th International Conference on Ferrites, 21DP1-2, Kyoto, Japan, Sept. 2000*.
109. J. G. Boerekamp, D. J. Huisman, and E. G. Visser "Improved ferrite for DSL application", *8th International Conference on Ferrites, 19Aa11-3, Kyoto, Jpn, Sept. 2000.*
110. "The use of ferrites in DSL wide band transformers", *FERROXCUBE, Application Note*, Sept. 2000, Eindhoven, The Netherlands.
111. D. J. Huisman, "Materials and core shape requirements for power applications", *Proceedings of MMPA users conference*, Sept. 1997, Chicago.
112. "Design of CCFL Backlight Inverters with Frame & Bar Cores", *FERROXCUBE, Application Note*, Eindhoven, The Netherlands, January 2003.
113. T. Mitsui and G. Van Schaick, *Powertechn. Mag.* **15** (Feb. 1991).
114. W. Waanders and A. Shpilman, *Powertechn. Mag.* **20** (May 1991).
115. D. J. Huisman, "Fast Design of planar SMPS transformers", *Proceedings of PCIM' 97*, Hong Kong, October 1997.
116. "New ER cores for Planar converters", *FERROXCUBE, Technical note*, Eindhoven, The Netherlands, Sept. 2002.
117. P. Gaudry and J. J. Putigny, *Electro. Puissance* **32**, 54 (1989).

118. "3C93, the new high temperature low loss power ferrite", *FERROXCUBE, Technical note*, Eindhoven, The Netherlands, May 2002.
119. "3C92, the new high saturation power ferrite", *FERROXCUBE, Technical note*, Eindhoven, The Netherlands, May 2002.
120. D. J. Huisnan and E. de Jong, "Design method for (ferrite) power inductors", *Proceedings of PCIM China 2003*, Shanghai, March 2003.
121. J. G. W. West, Permanent magnet materials, *IEE Seminars* 2000 and 2002.
122. Data on commercial ferrite Magnets (FXD grades): www.carbonelorraine.com.
123. M. McCraig and A. E. Clegg, *Permanent Magnets in Theory and Practice*, Pentech, London, 1987.
124. A. Mohr and J. Koch in Ref. 51, Pt. II, p. 515.

GENERAL REFERENCES

J. D. B. Veldkamp and R. J. Klein Wassink, *Philips Res. Rep.* **31**, 153 (1976).
A. B. D. van der Meer, *Sci. Ceram. Ned. Ker. Ver.* **9**, 535 (1979).
G. de With and N. Hattu, *Proc. Brit. Ceram. Soc.* **32**, 191 (1982).
M. Inasa, E. C. Liang, R. C. Bradt, and Y. Nakamura, *J. Am. Cer. Soc.* **64**, 390 (1981).
G. Cryssis *High Frequency Switching Power Supplies*, Mc. Graw-Hill Book Co., Inc., New York, 1984.
S. Mulder, *Application Note on the Design of Low Profile High Frequency Transformers? A new Tool in SMPS*, Philips Components, Eindhoven, The Netherlands, 1990.

FRANS KOOLS
Technology University
P. J. VAN DER VALK
Ferroxcube